Quasi-Distributed Fibre-Optic Chemical Sensing Using Telecom Fibre

By

Vincent James Murphy B.Sc. (Hons)

Submitted for the degree of Masters of Science

Presented to

Dublin City University

Research Supervisor

Dr. Brian MacCraith,

School of Physical Sciences,

Dublin City University,

February 1997

ACKNOWLEDGEMENTS

I would like to thank the following people who through their friendship, assistance or both made the last two years and a bit in DCU much more enjoyable.

Firstly, my supervisor Dr. Brian MacCraith for giving me the opportunity of doing this masters and for his support and guidance throughout. Many thanks to present and past members of the optical sensors group, especially Tom, Aidan, Aisling and Penny.

Thanks also to Alan Hughes, Al Devine, Des Lavelle, Charles Markham and Steve Coakley for their assistance when called upon.

For keeping me sane, thanks to the Tuesday and Thursday regulars in the sports complex and Eilish for the odd game of pool.

And finally, a special thanks to Oonagh, for not dumping me when I moved to a house with sky sports.

To my parents and Oonagh:
for whose support I am
indebted

ABSTRACT

A novel sensing approach combining sol-gel technology and standard graded index telecommunications fibre is presented. The tip of telecommunication fibre is etched using hydrofluoric acid resulting in a parabolic shaped cavity characteristic of the refractive index profile of the fibre. This cavity is then filled with sol-gel-derived silica doped with an analyte-sensitive dye. This configuration is evaluated using both fluorescence and absorption-based indicators for sensing chemical species such as oxygen and ammonia. The compatibility of the immobilisation system on telecommunications fibre with semiconductor laser diode excitation makes this approach particularly suited to quasi-distributed sensing. Preliminary results for multi-point pH sensing incorporating an 850nm Optical Time Domain Reflectometer and a near-infra-red dye are presented. The characterisation of a new family of materials known as organically modified silicates (Ormosils) is also carried out. Film thickness and temporal stability are monitored as a function of organic : inorganic precursor ratio while film microstructure is examined using FTIR spectroscopy.

TABLE OF CONTENTS

CHAPTER 1

INTRODUCTION

1.1 INTRODUCTION

Optical techniques for chemical sensing purposes have been developed for many application fields such as environmental and pollution monitoring, industrial process control and medicine. The working principle of an optical chemical sensor is based on the modulation of one of the optical properties (e.g. intensity, wavelength, phase, polarisation state) by the parameter under investigation. This modulation can occur via a variety of processes such as fluorescence, absorption, reflection, or scattering. Ideally the sensor should be capable of continuously and reversibly recording the presence and concentration of a particular species and should provide a usable output, generally in the form of an electrical signal, within a couple of seconds. Chemical sensing using optical techniques has the potential to overcome many of the problems associated with other measurement techniques such as electrical interference, cost and sensor size. Moreover, through the incorporation of fibre optics, remote and distributed sensing is feasible. Consequently, there is at present considerable interest in producing optical sensors for a wide range of chemical parameters to fulfil an ever increasing number of applications.

1.2 FIBRE OPTIC SENSORS

Over the last three decades optical methods have been used increasingly for sensing chemical analytes. The applications of these sensors are often enhanced when a bulk-optic configuration is replaced by fibre-optic technology. In the last few years the market for fibre-optic sensors (FOS) has grown considerably. The development of the field has undoubtedly been accelerated by the continuing growth of the optoelectronics industry. Currently, LEDs (Light Emitting Diodes) cover the visible spectrum from 400 to 700nm with some also available in the near infrared (NIR) and Mid-IR. Furthermore, laser diodes, which in many applications can replace

more expensive and bulky lasers, are soon expected to be available for the blue/green region of the visible spectrum. It is in this area of the spectrum that the absorption spectra of most current day indicators lie. However, the inherent characteristics of optical fibres is perhaps the main reason for the considerable interest in fibre optic sensors. Optical fibres are suitable for sensor systems for a number of reasons[1],

- *Geometrical versatility*: the flexibility, lightness and size of optical fibres facilitate highly localised measurements, for example, biomedical applications such as analysis of living cells and arteries.
- *Suitable material:* the fibre material (glass or plastic) is non-toxic and biocompatible. Furthermore the low attenuation of this material facilitates remote and distributed sensing.
- *Signal immunity*: since the primary signal is optical, it is not affected by electrical or magnetic fields.
- *Intrinsic safety*: due to the low light power used for sensing purposes, optical sensors do not present a risk of sparking, and are therefore suitable for use in potentially explosive areas e.g. mining and petroleum industries

The basic working principle of an intensity-based fibre-optic chemical sensor is shown in figure 1.1. The sensor may be intrinsic or extrinsic depending on whether the

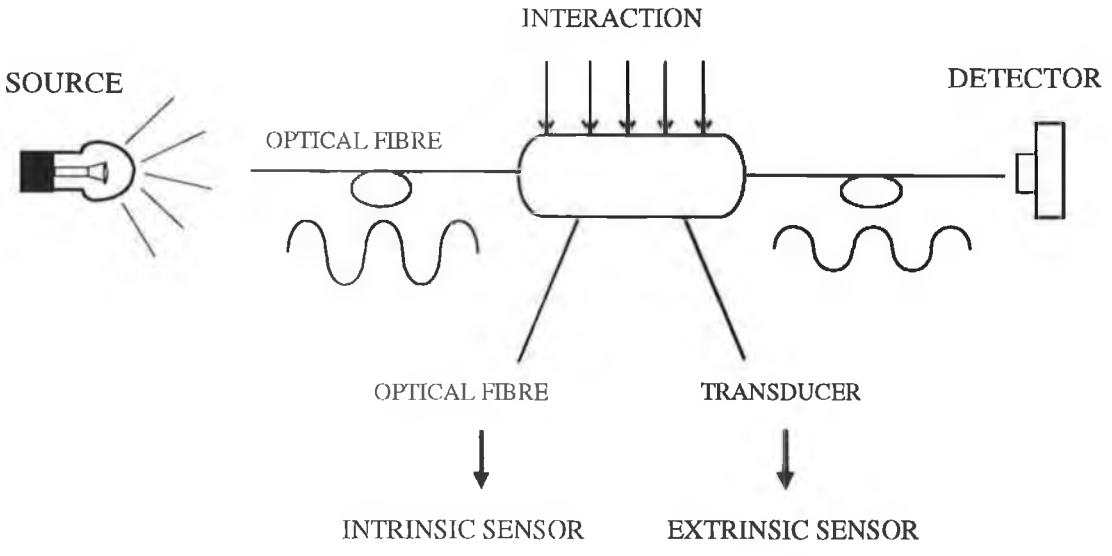

Figure 1.1 Working principle of an intensity-modulated fibre-optic sensor

intensity modulation is produced within the fibre or by an external transducer connected to the fibre. Generally fibres having diameters larger than 100μm are used to maximise the sensors coupling efficiency to the excitation source. The source can be either lamps, lasers, LEDs or laser diodes while the detector is generally a PIN-type photodiode. The concentration of the analyte under investigation is determined by monitoring the throughput of the fibre. In this work, both step index and graded-index fibres were used in fluorescence intensity-based intrinsic fibre-optic sensors for the measurement of carbon dioxide, pH and oxygen.

1.3 QUASI-DISTRIBUTED SENSING

The use of optical fibres as a support structure for chemically-sensitive dyes offers the potential for fully distributed or quasi-distributed multipoint sensing. This could be achieved by coating a fibre along its total length during drawing or by splicing in sensing regions. In such a way, both the concentration and position of a measurand can be determined simultaneously. For many industrial and environmental applications, a distributed or at least quasi-distributed sensor network is required rather than individual measuring devices. While this aim could be fulfilled by electrically interfacing a number of individual sensors, a quasi-distributed sensing system using a fibre-optic network offers a number of operational advantages. Obvious advantages include the reduced cost, ease of multiplexing and the system's immunity to electrical and magnetic interference. Furthermore, the low fibre attenuation along with the availability of fibre-optic couplers makes optical fibres ideally suited for this application. While a number of mechanisms to optically combine individual sensors has been explored, such as wavelength division and frequency division multiplexing[2], time division multiplexing has received most attention. In time division multiplexing, short pulses (ns or less) from generally a laser diode are used to interrogate the sensor network. The various sensing points along the fibre are then distinguished by monitoring the reflected signal as a function of time. This technique known as Optical Time Domain Reflectometry is widely used in the telecommunications industry for measuring the attenuation of optical fibres along their length.

1.3.1 Background to distributed sensing

Despite the potential benefits of a distributed fibre optic sensing system and the significant research that has been carried out in this area[3], very few distributed fibre optic sensors (DFOS) have so far appeared in the commercial marketplace. Of those commercially available, they are almost exclusively concerned with distributed temperature sensing. The working principle of a distributed optical fibre temperature sensor (DTS) was first demonstrated in 1981 at Southampton University using techniques derived from telecommunications cable testing. Subsequent work at *York Technology UK*, started in 1984, resulted in the first DTS prototype[3]. The sensor works because the local light scattering power of a fibre core strongly depends on the fibre temperature. When a sample such as a silica matrix is irradiated with a pulse of light of higher frequency (higher energy) than would correspond to any electronic transition, the majority of the light passes through the sample without attenuation but a small fraction is scattered giving rise to very faint lines corresponding to transitions between vibrational levels. The scattered spectrum known as the Raman spectrum consists of a centrally situated Rayleigh line and a series of less intense lines located either side of the central line known as Stokes and Anti-Stokes lines. The temperature profile of the fibre is determined from the relationship between these two series of lines using the following relationship

$$\frac{I_{as}}{I_s} \propto \exp\left(-\frac{hc\nu}{kT}\right)$$

where I_{as} and I_s correspond to the intensities of the Anti-Stokes and Stokes light respectively. T is the absolute temperature, h is Planck's constant, c is the speed of light, ν is the Raman shift in cm^{-1} and k is Boltzmann's constant. A spatial resolution of 1m over 10km and a temperature resolution of +/- 1^0C over the temperature range -140^0C to +460^0C was achieved with typical response times of 5 to 10 seconds. Fire detection and power cable monitoring are perceived to be the biggest markets for this sensing technique at present.

A number of distributed strain and pressure sensing systems are now also commercially available. *Herga Electric UK* has produced a range of pressure sensitive safety mats[3]. The mat is a microbend type sensor using Hergalite fibre, a large core multimode fibre with a hard acrylic spiral overwind. When a load is

introduced onto the mat, light is coupled out of the fibre depending on the weight of the load. The sensor is seen to have applications mainly in industrial process control. *G2 Systems Corporation(USA)* have developed a range of distributed sensors for use in monitoring cracks and deformations in concrete structures[3]. As with the pressure sensitive mat, the strain in the structure under investigation is deduced from the attenuation of the fibre in the sensing region.

The use of optical fibres for distributed sensing of gaseous and liquid chemical species is likely to be the most important application of this technology. As a result, the field is presently the subject of intense research activity[4]. Whilst there is undoubtedly a large number of potential markets in this sector, this research has yet to reach the commercial prototype stage.

1.4 THE SOL-GEL PROCESS

In the area of fibre optic chemical sensing, a method of immobilising analyte-sensitive reagents onto the sensing fibre is required. The potential of sol-gel derived materials for this application has generated considerable research activity. The sol-gel process is a method by which glasses and ceramics can be fabricated at low temperatures through the hydrolysis and polymerisation of alkoxide precursors[5]. Figure 1.2 illustrates the main steps of the process. The process typically involves a solution consisting of a metal alkoxide, water which acts as the hydrolysis agent, alcohol as solvent and either an acid or base as catalyst. These are mixed together to achieve chemical homogeneity on the molecular scale. At low temperatures (<100°C), the metal compounds undergo hydrolysis and polycondensation to produce a sol in which fine particles (colloids) are dispersed. Further reaction connects the particles to produce a disordered branched network which is interpenetrated by liquid. Low temperature curing removes any of the remaining solvents and leaves the porous oxide. Further solidification of the gel by means of high temperature annealing gives rise to monolith glasses and ceramics. This process is widely used in sensing applications to produce supports for analyte-sensitive species. Through the appropriate selection of the process parameters, microporous films can be coated onto optical fibres or glass slides. The dye molecules, which are added at the start of the process become entrapped in the pores of the sol-gel material in nanometre-scale cage - like structures

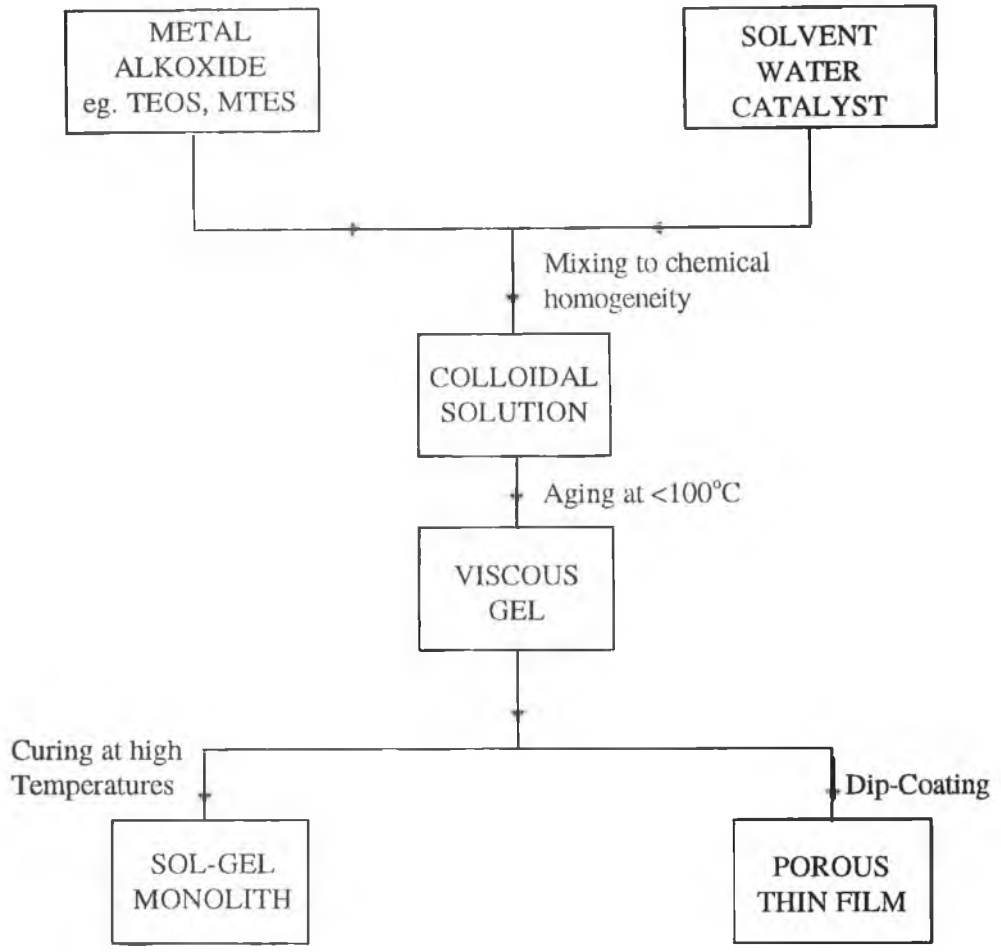

Figure 1.1 **Schematic diagram of the sol-gel process**

which are accessible to smaller analyte molecules which permeate the silica network[5]. One of the main advantages of the sol-gel method over other coating techniques is the flexibility it presents to the user. Film parameters such as porosity, thickness, and hydrophobicity can all be easily optimised through appropriate changes to the sol-gel process parameters. Furthermore, the sensor fabrication is simple and inexpensive as it involves a straight-forward dip-coating of the substrate followed by curing at room temperatures. In this work, the sol-gel method is used to produce supports for a range of indicator dyes for use in evanescent wave and direct excitation-based sensors.

1.5 THESIS OBJECTIVES AND OUTLINE

The main objectives of this project were as follows:

- Investigation of the properties of organically modified silicates (ormosils)
- Development of a sol-gel immobilisation technique on telecom type optical fibre
- Evaluation of the possibility of using this technique in a quasi-distributed chemical sensor.

Chapter 2 of this thesis outlines the different methods used in our laboratory for characterising sol-gel-derived thin films, namely Ellipsometry, Spectral transmission and Fourier Transform Infrared (FTIR) Spectroscopy. These methods are used to characterise a relatively new family of materials known as ormosils. Chapter 3 describes the development of a fibre optic carbon dioxide sensor based on evanescent wave excitation of a pyranine complex entrapped by a thin microporous coating fabricated by the sol-gel process. The sensor is based on the quenching of fluorescence from the indicator molecules in the presence of carbon dioxide. Chapter 4 deals with the encapsulation of analyte indicators onto telecommunications fibre for point sensing applications. The sensor is based on selective fibre etching and sol-gel immobilisation. Sensor evaluation is carried out using both absorption and fluorescence-based indicator dyes. Finally, chapter 5 examines the possibility of using this immobilisation technique in a quasi-distributed chemical sensor system. A number of absorption-based sensing fibres are fusion coupled onto a sensor network. An optical time domain reflectometry technique is then used to discriminate between the reflected light signals from the various sensing regions.

REFERENCES

1. A.G. Mignani, F. Baldini **"Biomedical sensors using optical fibres"** Prog. Phys. 59 (1996), pp.1-28.

2. J.M. Senior, S.E. Moss, S.D. Cusworth. **"Wavelength division multiplexed optical point-sensor networks using injection laser diode sources"** Optics & Laser Technology 28 No. 1 (1996), pp.1-5.

3. S.D. Crossley. "**Commercial prospects for distributed fibre optic sensors**" Optical Sensors Collaborative Report (UK) Contract 102, (1992).

4. **Distributed and Multiplexed Fiber Optic Sensors Vi** SPIE 2838, (1996).

5. B.D. MacCraith, C.M. McDonagh, G. O'Keeffe, A.K. McEvoy, T. Butler, F.R. Sheridan. **"Sol gel coatings for optical chemical sensors and biosensors"** Sensors and Actuators B 29 (1995), pp.51 - 57.

CHAPTER 2

SOL GEL THIN FILM CHARACTERISATION

2.1 INTRODUCTION

With the increasing interest in sol-gel coatings for sensing applications[1,2], appropiate methods of investigating the properties of thin films are important. Parameters of significance include the film thickness, refractive index, porosity and optical quality. For example, the response time of a sensor is a function of the sensing film porosity and thickness, while the refractive index is a fundamental parameter for waveguide applications. In this chapter, two methods of determining the refractive index and thickness of sol-gel derived thin films are presented, namely Ellipsometry and Spectral transmission. Fourier Transform Infrared (FTIR) spectroscopy was also employed to provide information on the chemical structure of the films. Film properties were monitored using the above techniques, and the results were interpreted in terms of the chemical reactions involved in the sol-gel process.

2.2 SOL GEL DERIVED THIN FILMS

The main reaction components involved in a typical sol-gel process are a metal alkoxide such as Tetraethylorthosilicate (TEOS), water, a mutual solvent (typically ethanol) and a catalyst (HCl). These are mixed thoroughly to achieve homogeneity on a molecular scale, followed by ageing at a fixed temperature. During this period, through the hydrolysis and condensation of the alkoxide precursor, a polymeric SiO_2 network is formed in the solution. Hence the sol-gel process is the transition of a system of colloidal particles (sol) in a solution, into a disordered, branched, continuous network (gel), which is interpenetrated by liquid. After a suitable ageing period, the solution becomes viscous enough for the fabrication of sol-gel thin films by means of dip-coating or spin-coating techniques. The dip coating technique, used in this work, is most widely applied for sensing purposes, due to the diversity of substrates that can be

employed. In this work, sol-gel thin films were deposited onto both planar (silicon wafers or glass slides) and optical fibre substrates using this coating technique. In dip coating, the prepared[3] substrate is immersed into the sol gel solution and then withdrawn at a constant controlled speed. In our laboratory, the substrate is held rigid in a draft and vibration free environment, while the solution, on a vertically moveable platform, is drawn away from the sample. A schematic diagram of the apparatus used is shown in figure 2.1. During withdrawal, a thin film (100nm - 1μm) becomes entrained on the substrate. The thickness of this film is dependent on a number of factors, including withdrawal speed. withdrawal angle, coating solution viscosity and the substrate adherence. Although the interdependence of the various process parameters is complex, the film thickness is given approximately by the following relationship,[4]

$$\text{thickness} = \left(\frac{\text{Withdrawal speed} \times \text{Viscosity}}{\text{Solution density}}\right)^{\frac{2}{3}}$$

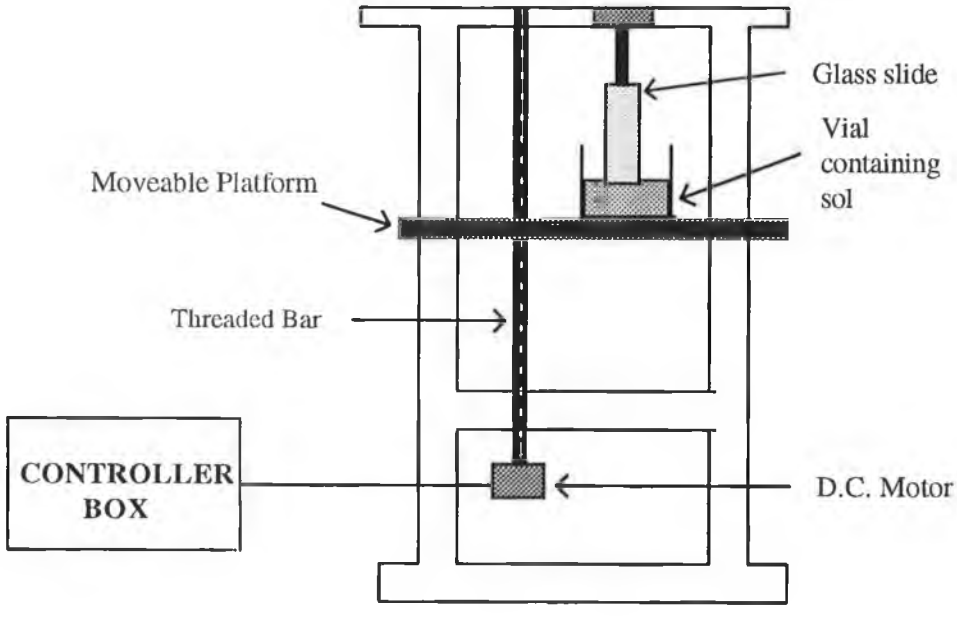

Figure 2.1 Dip-coating apparatus

Therefore, thicker coatings are achieved at faster withdrawal rates, i.e. for the same solution, the film thickness is proportional to the withdrawal speed to the power of 0.66. After coating, the films can be densified as needed by drying in an oven or at room temperature.

2.3 THIN FILM CHARACTERISATION METHODS

2.3.1 Introduction

The following sections outline the techniques used in our laboratory for measuring the thickness and refractive index of sol-gel-derived films. These techniques are ellipsometry and spectral transmission. The accuracy and limitations of the two methods are discussed

2.3.2 Ellipsometry

When light of a particular state of polarisation is reflected from an interface between two optically dissimilar media, such as a sol gel thin film on a silicon substrate, its polarisation state is modified [5]. Ellipsometry is simply the measurement and interpretation of this change of polarisation.

The ellipsometer used in this work was a Rudolph Research AutoEL-III which is a nulling ellipsometer. A schematic diagram of the ellipsometer arrangement is shown in fig 2.1. A collimated monochromatic beam from a HeNe laser is passed through the variable polariser to produce a light beam of known controlled polarisation. This light interacts with the thin film under investigation and its polarisation state is modified. The reflected light is then passed through the analyser and onto a photodetector. The polariser and analyser are now rotated until the intensity of the reflected beam is at a minimum. The angles of the polariser and analyser are then determined. These angles at null are convertible by means of linear equations[6] into the polarisation parameters[6] Δ and Ψ, which are related by

$$\rho = \tan\Psi \, e^{(i\Delta)}$$

where ρ is the ratio between the reflection coefficients r_p and r_s, p and s refer to the two orthogonally linearly polarised components of the reflected beam.

The parameters Δ and Ψ are functions of the incident angle, the thickness of the thin film and the refractive indexes of the surrounding medium, thin film, and substrate. Since some of these parameters are known, this enables the software within the ellipsometer to calculate the thin film thickness and refractive index. However, when the optical path length of the light traversing the film reaches an integral number of wavelengths, Δ and Ψ are the same for successive integral path length multiples. In other words Δ and Ψ are cyclic functions of the film thickness. Therefore the actual thickness of the film could be the zero order thickness + any integer times the full cycle thickness (ordinate). Because of this cyclic behaviour, an additional method of corroborating the film thickness is required. This method will be discussed in the next section.

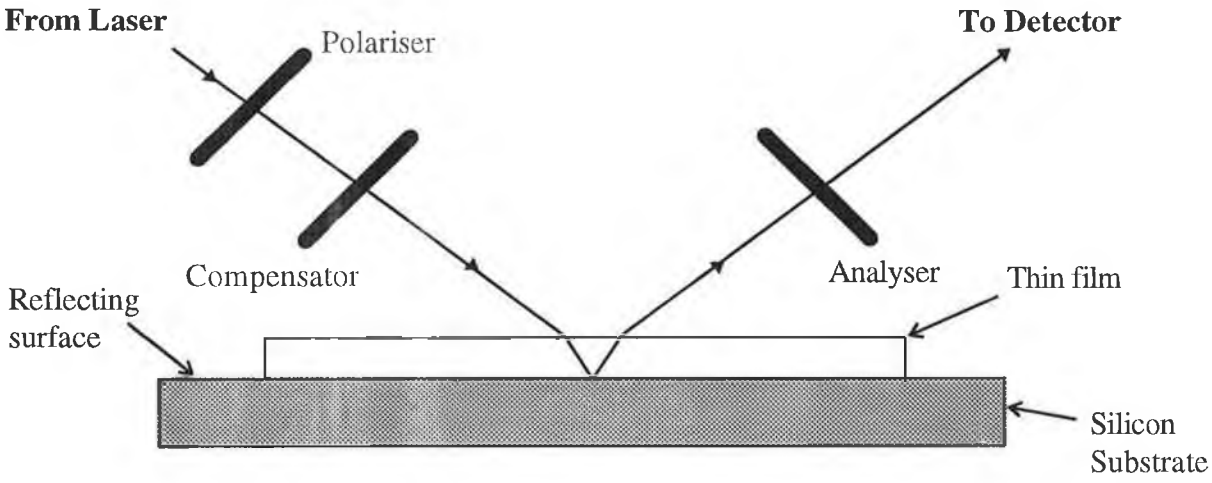

Fig. 2.1 **Schematic diagram of ellipsometer**

2.3.3 Spectral Transmission

The refractive index and thickness of sol-gel thin films can also be determined, although with less accuracy, by analysing the transmission spectra of the films over the wavelength range 350-1200nm[7]. The analysis presented here is based on the reflectance and transmittance of light by a single non-absorbing film coated onto both sides of a non-absorbing glass substrate, as shown in fig 2. Each time the light strikes an interface, the beam is divided into reflected and transmitted parts. The final transmission or reflectance intensity is then obtained by summing the individual reflected or transmitted elements. To simplify this summation we consider the case for a single layer of thickness d and refractive index n_1 coated onto an infinite glass substrate(i.e. no reflectance from the back of the slide) as shown in fig. 2.3. In this case, the amplitudes of successive beams reflected from the glass substrate are represented by r_{01}, $t_{01}t_{10}r_{12}$, $t_{01}t_{10}r_{10}r_{12}^2$

The change in phase δ_1 of the beam in traversing the film is given by

$$\delta_1 = \frac{2\pi}{\lambda} n_1 d \, Cos\phi_1 \qquad \text{eqn. 2.1}$$

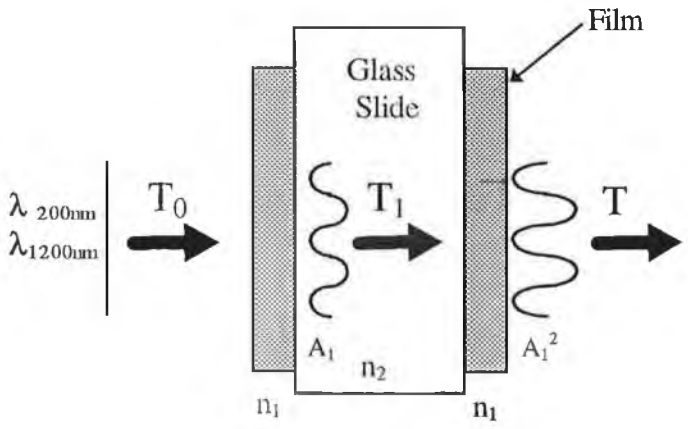

Fig 2.2 Double sided sol-gel coated slide used in spectral transmission analysis

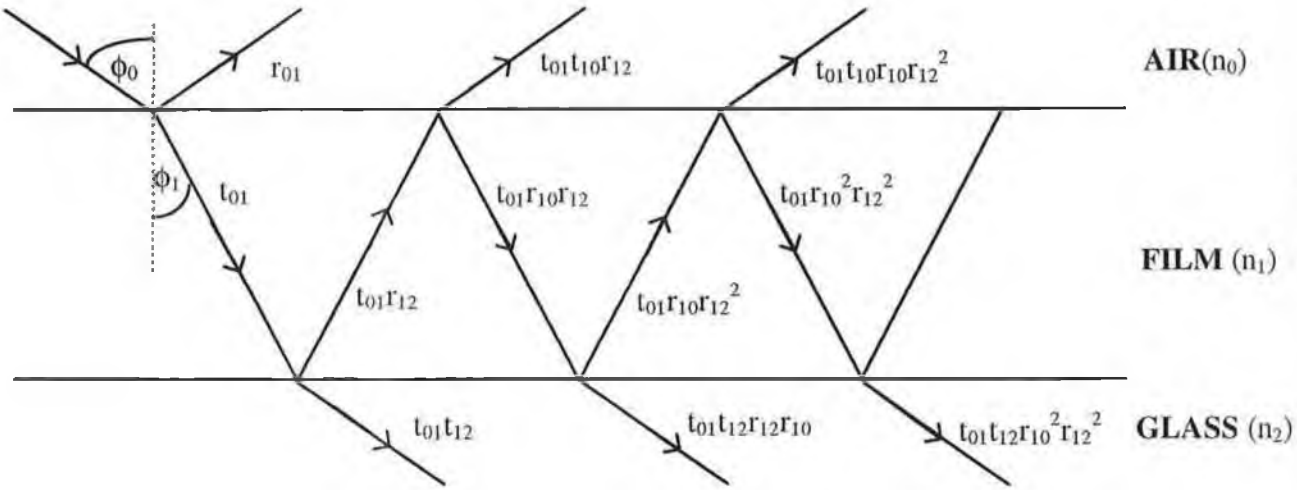

Fig. 2.3 **Reflectance and transmittance of light from a single film coated onto an infinite substrate**

The reflected amplitude is thus given by

$$R = r_{01} + t_{10}t_{01}r_{12}e^{-2i\delta_1} - t_{10}t_{01}r_{10}r_{12}^2e^{-4i\delta_1} + \ldots\ldots \qquad \text{eqn. 2.2}$$

Using the sum of the series $s_\infty = \frac{s_1}{1+r}$, this summation yields

$$R = r_{01} + \frac{t_{10}t_{01}e^{-2i\delta_1}}{1 + r_{01}r_{12}e^{-2i\delta_1}} \qquad \text{eqn 2.3}$$

From conservation of energy and remembering that $r_{01} = -r_{10}$, it can be shown (Stokes law) that

$$t_{01}t_{10} = 1 - r_{01}^2 \qquad \text{eqn. 2.4}$$

and therefore equation 2.3 reduces to

$$R = \frac{r_{01} + r_{12}e^{-2i\delta_1}}{1 + r_{01}r_{12}e^{-2i\delta_1}} \qquad \text{eqn 2.5}$$

where R represents the total amplitude of the reflected beams. The corresponding intensity is given by

$$R_{tot} = R.R^* = \frac{r_{01}^2 + r_{12}^2 + 2r_{01}r_{12}Cos2\delta_1}{1 + r_{01}^2r_{12}^2 + 2r_{01}r_{12}Cos2\delta_1} \qquad \text{eqn. 2.6}$$

where

$$r_{01} = \frac{n_0 - n_1}{n_0 + n_1}, \qquad r_{12} = \frac{n_1 - n_2}{n_1 + n_2} \quad \text{for normal incidence.} \qquad \text{eqn 2.7}$$

From equations 2.1 and 2.6, it can be seen that maxima and minima of the reflectance curve occur at values of n_1d given by

$$n_1d = (2m+1)\lambda/4, \qquad n_1d = (2m+2)\lambda/4 \quad \text{respectively.} \qquad \text{eqn. 2.8}$$

For the case where the refractive index of the coating is greater than the refractive index of the substrate i.e. $n_1 > n_2$, the value of reflectances at these points is given by

$$R_{\min} = \left(\frac{r_{01} + r_{12}}{1 + r_{01}r_{12}}\right)^2 = \left(\frac{n_2 - n_0}{n_2 + n_0}\right)^2 \qquad \text{eqn. 2.9}$$

$$R_{\max} = \left(\frac{r_{01} - r_{12}}{1 - r_{01}r_{12}}\right)^2 = \left(\frac{n_1^2 - n_0n_2}{n_1^2 + n_0n_2}\right)^2 \qquad \text{eqn. 2.10}$$

Since the sum of reflectance and transmittance must equal 1, the light intensity transmitted into the glass substrate(fig 2.1) is represented by

$$T_{(1)\max} = 1 - \left(\frac{n_2 - n_0}{n_2 + n_0}\right)^2 \qquad T_{(1)\min} = 1 - \left(\frac{n_1^2 - n_0 n_2}{n_1^2 - n_0 n_2}\right)^2 \qquad \text{eqn. 2.11}$$

At this stage, the light has traversed an AIR-FILM-GLASS path. On exiting the slide the light undergoes the reverse path i.e. GLASS-FILM-AIR. It can be shown from equation 2.11 that the analysis for these two paths are identical. Therefore

$$T_{\max} = T_{(1)\max}^2 = \left[1 - \left(\frac{n_2 - n_0}{n_2 + n_0}\right)^2\right]^2 = \frac{2n_2}{n_2^2 + 1} \qquad \text{eqn. 2.12}$$

$$T_{\min} = T_{(1)\min}^2 = \left[1 - \left(\frac{n_1^2 - n_0 n_2}{n_1^2 + n_0 n_2}\right)^2\right]^2 \qquad \text{eqn. 2.13}$$

It is apparent from the above equations, that the refractive index of the film (n_1) can be related to the difference between the maximum and minimum transmission values i.e.

$$\Delta T = \frac{2n_2}{n_2^2 + 1} - \left[1 - \left(\frac{n_1^2 - n_0 n_2}{n_1^2 + n_0 n_2}\right)^2\right]^2 \qquad \text{eqn. 2.14}$$

Similarly, for the case where the refractive index of the coating is less than the refractive index of the substrate i.e. $n_1 < n_2$

$$\Delta T = \left[1 - \left(\frac{n_1^2 - n_0 n_2}{n_1^2 + n_0 n_2}\right)^2\right]^2 - \frac{2n_2}{n_2^2 + 1} \qquad \text{eqn. 2.15}$$

To solve for n_1, a graph of ΔT versus refractive index between the values of 1.42 and 1.6 was plotted (fig 2.3). Values of 1 and 1.517 were substituted for the constants n_0 and n_2 in equations 2.14 and 2.15.

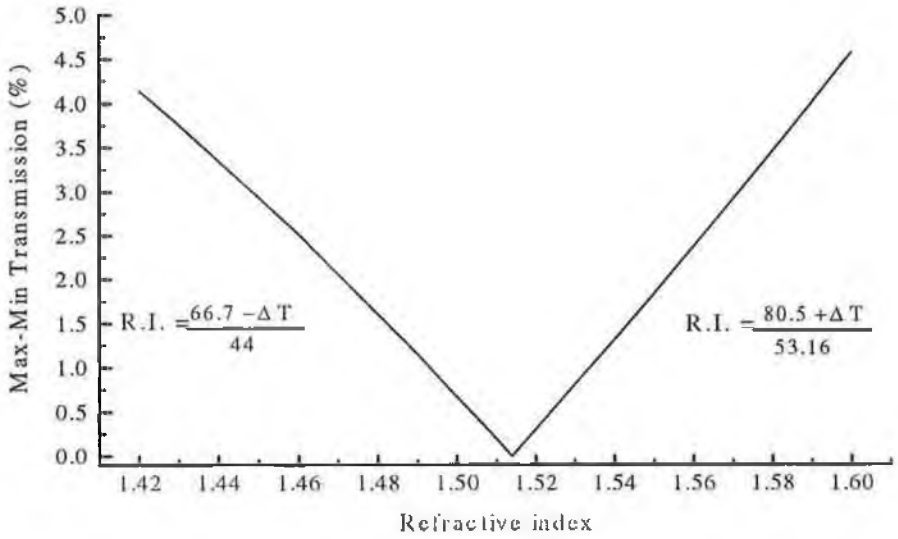

Fig 2.3 **Graph of max-min transmission versus refractive index for a double sided non-absorbing coating on a glass slide.**

The refractive index of the film under investigation can now be determined by simply substituting the max-min transmission value into the appropiate equation of the line shown in fig 2.3.

The film thickness can also be determined from the transmission spectra from the position of the interference maxima/minima. The basic condition for interference fringes is

$$2nd = m\lambda \qquad \text{eqn. 2.16}$$

From this it follows that the thickness is given by

$$d = \frac{\Delta m}{2n_1\left(1/\lambda_1 - 1/\lambda_2\right)} \qquad \text{eqn. 2.17}$$

where Δm is the order of separation between the extrema and λ_1, λ_2 are the wavelengths at the extrema of interest.

Sample transmission spectra of two sol gel thin films, one of refractive index less than the substrate and one greater, are shown in figures 2.4a and 2.4b. It should be noted that where possible

- An average of a number of extrema should be used to calculate ΔT
- Peaks outside the range 450-750nm should be ignored
- A large value of Δm should be used when calculating the film thickness.

Refractive index calculations using the spectral transmittance technique agreed (within 1%) with ellipsometry measurements. The spectral transmittance technique however has the advantage that it will yield refractive index values for any thickness of film above 300nm while refractive index measurements using the ellipsometer are limited to cases where the film thickness is between 1/5 and 4/5 the ordinate. However, it should be noted that the accuracy of the spectral transmittance method for refractive index measurements reduces significantly both with decreasing film thickness and decreasing refractive index differential between the coating and glass substrate. As a result, the accuracy of the spectral transmittance method for determining the refractive index of sol-gel films is realistically an order less than ellipsometry measurements.

Thickness measurements using the two methods however failed to agree. On average sol-gel films were observed to be between 5 to 15 % thicker on glass substrates. Therefore, the spectral transmittance method can not be used to verify ellipsometer thickness measurements. However the technique can still be used to remove the uncertainty in ellipsometry measurements (i.e. the number of ordinates to be added). The two methods together can thus be used to determine the thickness of any sol-gel film.

Finally, it should be noted that this analysis is limited to cases where the thickness of the

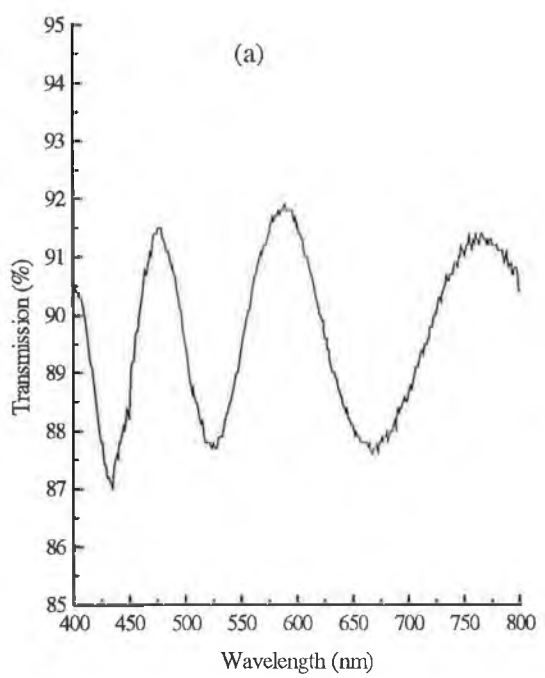

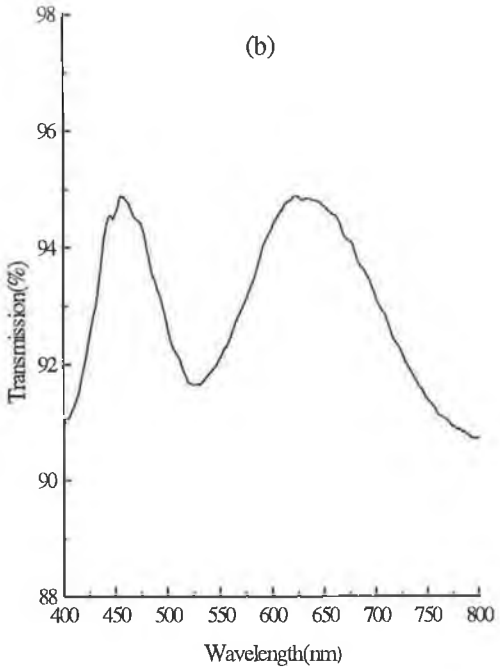

$$RI = \frac{80.5 + 4.5}{53.2} = 1.598$$

$$t = \frac{2}{2*1.598\left(\frac{1}{467nm} - \frac{1}{764nm}\right)} = 752nm$$

$$RI = \frac{66.7 - 3.4}{44} = 1.438$$

$$t = \frac{1}{2*1.438\left(\frac{1}{456nm} - \frac{1}{635nm}\right)} = 636nm$$

Fig. 2.4 **Transmission spectra of a double sided sol-gel film coated glass substrate(a) $n_1 > n_2$, (b) $n_1 < n_2$. Also included are thickness and refractive index calculations for the two films.**

front film is identical (within 20nm) to the back film. In this case, the interference patterns from the two film-glass interfaces are in phase and can be summed easily. The analysis becomes considerably more difficult for dissimilar films.

2.4 ORGANICALLY MODIFIED SILICATES

2.4.1 Introduction

Ormosils (organically modified silicates) are a relatively new family of materials in which inorganic and organic components are linked by chemical bonds to form a non-crystalline network[8]. Because of this chemical bonding between the two constituents, unique properties can be obtained. In the case of mechanical properties, the introduction of the organic components induces flexibility and toughness, thereby reducing the brittleness of the inorganic network structure. In other words, the introduction of the organic components changes the properties of the material to be more polymer-like than glass-like. This enables the preparation of thick films without cracks. It has been observed that with sols prepared from Tetraethoxysilane (TEOS) and Methlytriethoxysilane (MTES), it was possible to achieve film thicknesses up to 2μm[9], compared to around 0.5 - 1μm with TEOS only. Furthermore, it has been shown that films prepared from MTES are less porous (a denser structure) than films prepared just from TEOS[9]. However, perhaps the most interesting feature of ormosils is the effect the organic groups have on the surface properties of the sol-gel films. The moisture sensitivity of sol-gel derived silica is a major obstacle for many sensing applications. The most straightforward solution to this, is to prevent water adsorption, by enhancing the hydrophobicity of the sensing surface through chemical means. The surface of TEOS-based films are characterised by a large concentration of hydroxyl (-OH) groups which readily interact with moisture in the film environment. By replacing these hydrophilic groups with hydrophobic methyl (CH_3) groups the affinity of the sensing surface to water vapour can be modified. This has been achieved in our laboratory[10] by introducing a range of organically modified alkoxide precursors to the sol gel process.

In the following section, the effects of the organic precursor on the long term stability of the sol-gel films are presented. The thickness and refractive index of the films are measured using the characterisation methods described in the previous section. The results are compared with those of TEOS based films.

2.4.2 Temporal behaviour of films

For applications in optical sensors, the long term stability of sol-gel derived thin films is a critical requirement. To this regard, there is considerable interest in producing films whose microstructure would remain constant over the working life of the sensor. Monitoring of the film thickness is one means by which the evolution of the film microstructure can be analysed. In figure 2.5, the temporal evolution of the film thickness for R=2 and R=4 TEOS films is shown[11], where R is the water : precursor molar ratio. It is clear from the data that the microstructure of these films continues to evolve for a considerable time after coating. This decrease in thickness is attributed to incomplete hydrolysis in the films even though R=2 is the stoichiometric water : TEOS ratio. Hydrolysis continues to occur after the drying step by interaction with moisture in the atmosphere, thereby resulting in a decrease in the film thickness. Thickness of films stored in the desiccator changed little from their original values over time, thus supporting this theory. In the case of the R=2 films, the thickness only starts to stabilise after 60 days. Thus, sensors using R=2 films would have to fabricated at least 2 months prior to their use

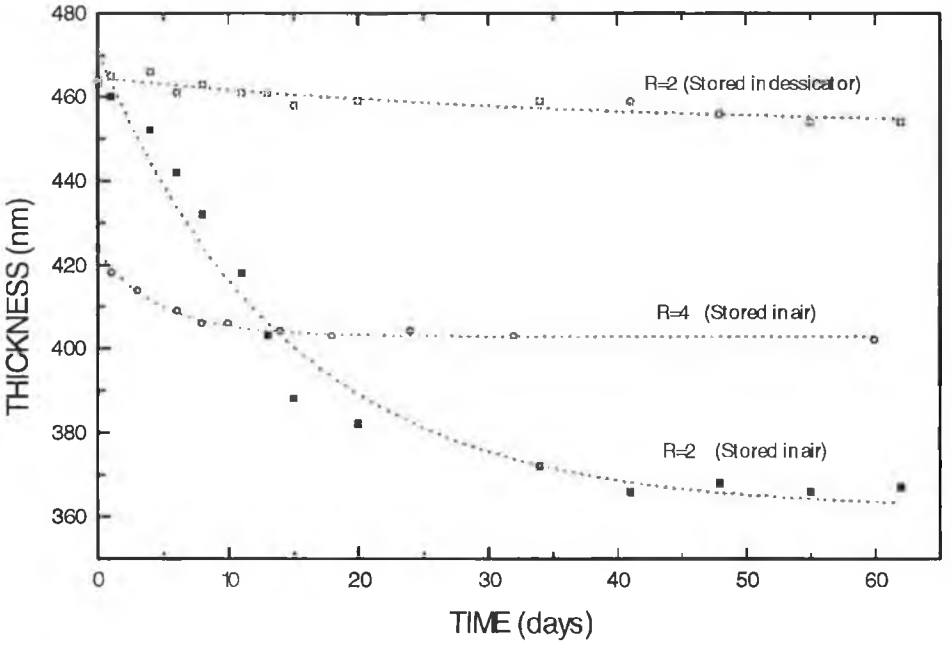

Fig. 2.5 Temporal evolution of film thickness for R=2 and R=4 TEOS films

to ensure a repeatable response as evolving film microstructure would be expected to have an effect on the sensor calibration.

In order to produce films with a quicker stabilisation time a combination of methyltriethoxysilane $CH_3Si(OC_2H_5)_3$ and tetraethoxysilane $Si(OC_2H_5)_4$ were used as precursors. Sols using different mixtures of these products (by weight) were made up using the following recipe: 6 g precursor, 4 g ethanol, water at pH1 using HCl as catalyst. The amount of water was varied depending on the desired R value. All films were doped with 40000ppm ruthenium for sensing purposes not dealt with here. The solution was stirred for 1 hour at room temperature. Coatings were then deposited onto cleaned soda-lime glass slides and silicon wafers using the dip-coating process described earlier.

Figure 2.6 shows the temporal evolution of the film thickness for an R=2, 1:1 ratio of MTES:TEOS film coated at 0.971mm/sec. The thickness decreases to a lesser extent than the R=2 TEOS film over the same time period, but still has not stabilised after 70 days. The MTES:TEOS ratio was now kept constant while the R value was increased.

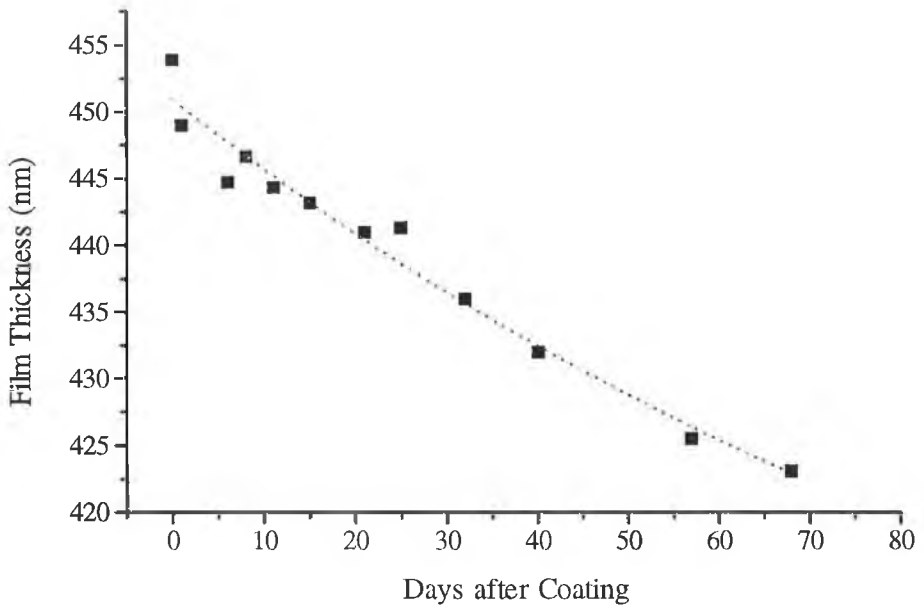

Fig. 2.6 Temporal evolution of film thickness for a 1:1 MTES:TEOS R=2 film

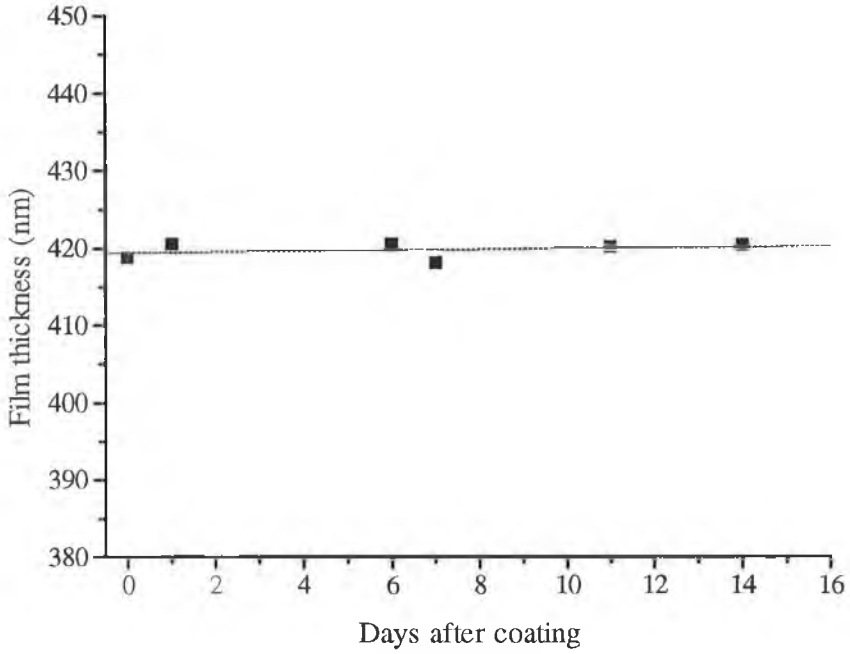

Fig 2.7 Temporal evolution of film thickness for a 1:1 MTES:TEOS R=4 film

Figure 2.7 shows the temporal evolution of the film thickness for an R=4 1:1 MTES:TEOS film over a period of 2 weeks. From these two graphs, it is clear that the organic precursor and R value play a significant role on reducing the film stabilisation time. As mentioned earlier, the use of an organic precursor such as MTES changes the surface properties of sol-gel silica films. The surface of TEOS-based films are characterised by a large concentration of hydrophilic -OH groups. When an MTES precursor is introduced, these groups are replaced with $-CH_3$ groups. Since $-CH_3$ groups are not affected by water, a permanent hydrophobicity is obtained. As a result, hydrolysis ceases to take place within the sol-gel microstructure, thus resulting in more stable films. In the next section, the use of FTIR spectroscopy to characterise these changes is reported.
All R=4 films with 50% or greater MTES content were found to stabilise within a day of coating. For R=2 films an MTES content of 75% was required to yield stable films.

Sol-gel films were also made up from a 1:1 (by weight) mixture of MTES and ethanol without any water[1]. The hydrolysis reaction was catalysed by adding 1% (w/w) of

concentrated HCl dropwise to the solution. After ageing for 24 hours, films were coated onto glass slides at 0.971mm/sec as before. This recipe also yielded extremely stable films of thickness ~ 390nm.

2.5 FTIR OF SOL GEL DERIVED THIN FILMS

Fourier Transform Infrared (FTIR) spectroscopy has for years proven to be a useful tool for studying the structure of sol-gel-derived films at the molecular level. In this section, the structure of TEOS and ormosil based films coated onto silicon wafers are studied over the spectral range 4000-500cm^{-1} using a *Bomem MB120* FTIR. The significance of the predominant features is explained. All spectra are a result of 50 scans at normal incidence with a resolution of 4cm^{-1}.

In figure 2.8, the FTIR spectrum of an R=4 TEOS-based sol-gel film is shown. The main features of interest in the spectrum are assigned, according to Innocenzi et al.[9], as follows: the dominant band near 1070 cm^{-1} is ascribed to antisymmetric stretching of the oxygen atoms along the Si-Si direction: the wide band at around 3400-4000 cm^{-1} is ascribed to molecular water (O-H stretching) with contributions from hydrogen bonded internal silanols (3640 cm^{-1}) and free surface silanols (3740cm^{-1}): the peak at 910-940 cm^{-1} is attributed to stretching vibrations of Si-OH or SiO^- groups. The Si-O-Si band at 1070 cm^{-1} is accompanied by a shoulder localised at around 1200 cm^{-1}. It has been suggested by Almeida and Pantano[12] that the intensity of this feature can be correlated with the porosity of the sol-gel film. The authors suggested that this component is activated by the sol-gel pores that scatter in all directions the normally incident IR light. This relationship was verified here by densifying the TEOS film shown in figure 2.8 at 300° C followed by a further heat treatment at 500 ° C. As predicted, the decrease in porosity with heat treatment coincided with a decrease in the strength of this shoulder. The ratios between the absorption of this shoulder and that of the main peak can thus give a qualitative appraisal of the change in porosity with thermal treatment or indeed process parameters. This approach was used to investigate the porosity of films as a function of MTES content. A shift in the position of the Si-O-Si band was also observed with changing temperature.

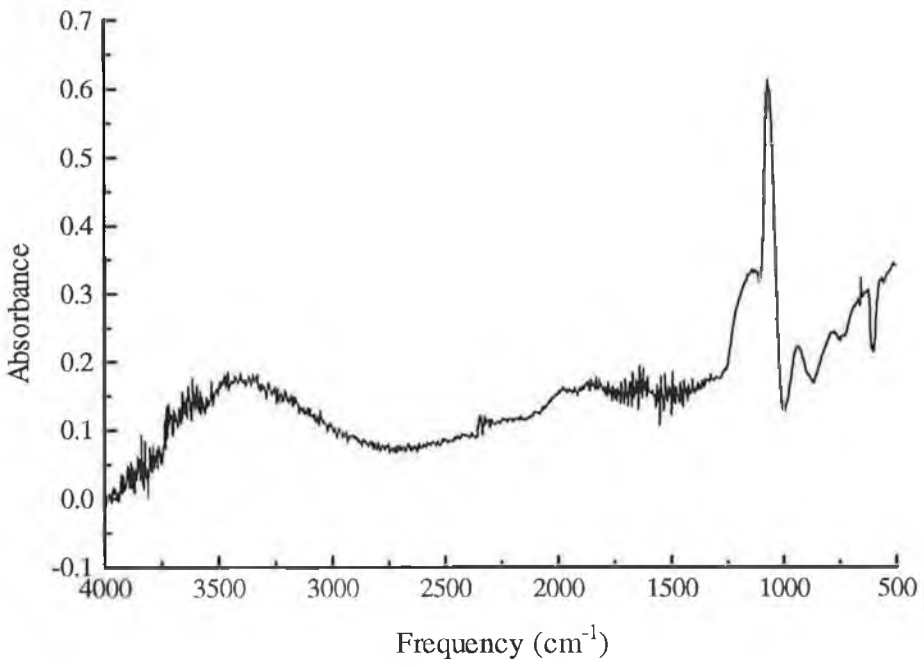

Fig. 2.8 FTIR spectrum of an R=4 TEOS-based sol-gel film

This band was observed to shift to lower frequencies (1070 to 1055cm^{-1}) with thermal treatment at 300° C, followed by a frequency increase at higher annealing temperatures. A similar observation was recorded by Almeida and Vasconcelos[13] for this feature. The intensity of the peaks at 910 cm^{-1} and 3400 cm^{-1} also decreased, as would be expected, with annealing temperature.

In figure 2.9 and 2.10 the FTIR spectrum of R=4, 1:1 MTES:TEOS and 100% MTES sol-gel films are shown. As mentioned earlier, MTES films are characterised by the presence of Si-CH_3 groups. These groups, which exhibit the absorption bands at 1260 cm^{-1} and 2900-3000 cm^{-1}, can be seen to increase with MTES content. However, the corresponding expected decrease in the Si-OH band at 910cm^{-1} with MTES content was not observed. A decrease in the intensity of the molecular water band at 3400 cm^{-1} with

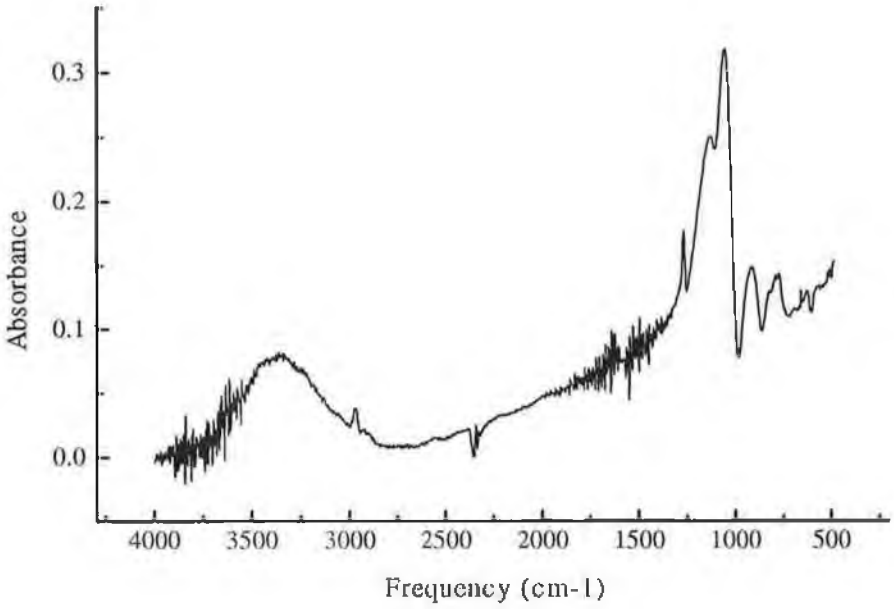

Fig. 2.9 FTIR spectrum of a R=4 1:1 MTES:TEOS sol-gel film

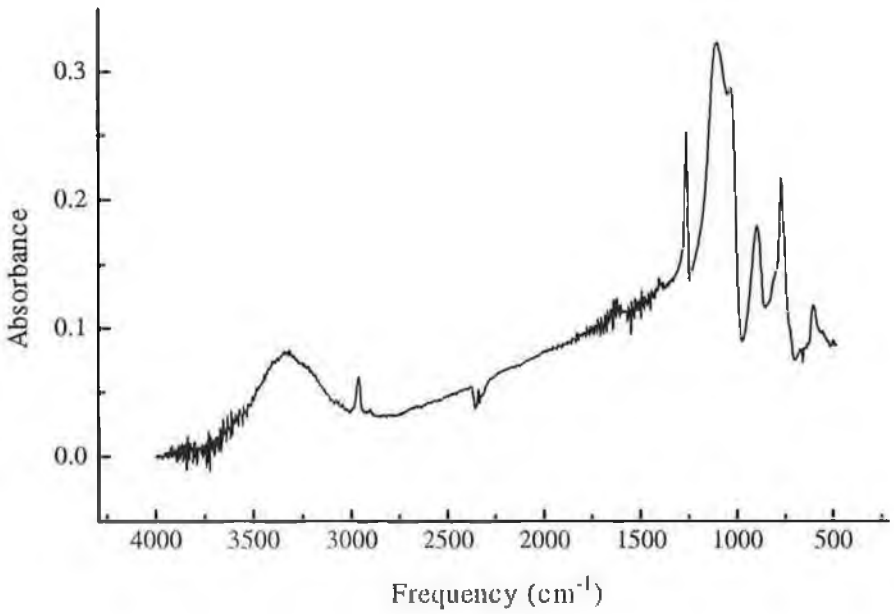

Fig. 2.10 FTIR spectrum of a MTES-based sol-gel film

MTES content was also predicted by Innocenzi et al. While this was not observed in our spectra, the contribution of the hydrogen and free surface silanols (3640 - 3740 cm^{-1}) was significantly reduced in the MTES films. Moreover, concerning the porosity of the ormosil based films, the ratio between the absorption of the Si-O-Si peak and that of the shoulder near 1200 cm^{-1} increased with the percentage of MTES. Thus, it may be deduced that the films prepared from MTES are less porous (i.e. more dense) than TEOS-based films. This is as expected, since the reduced porosity is in agreement with the higher flexibility and strength of the modified network as pointed out earlier.

FTIR spectra of sol-gel films prepared from the organic precursor ethlytriethoxy-silane (ETEOS) were also studied. In figure 2.11, the IR transmission of a 1:1 ETEOS: TEOS sol gel film is shown. A band near 3000 cm^{-1} representing the methyl groups is clearly evident. Furthermore there is a complete absence of the Si-OH band at ~ 900 cm^{-1} seen in the MTES and TEOS films. The contribution of the water band centred around

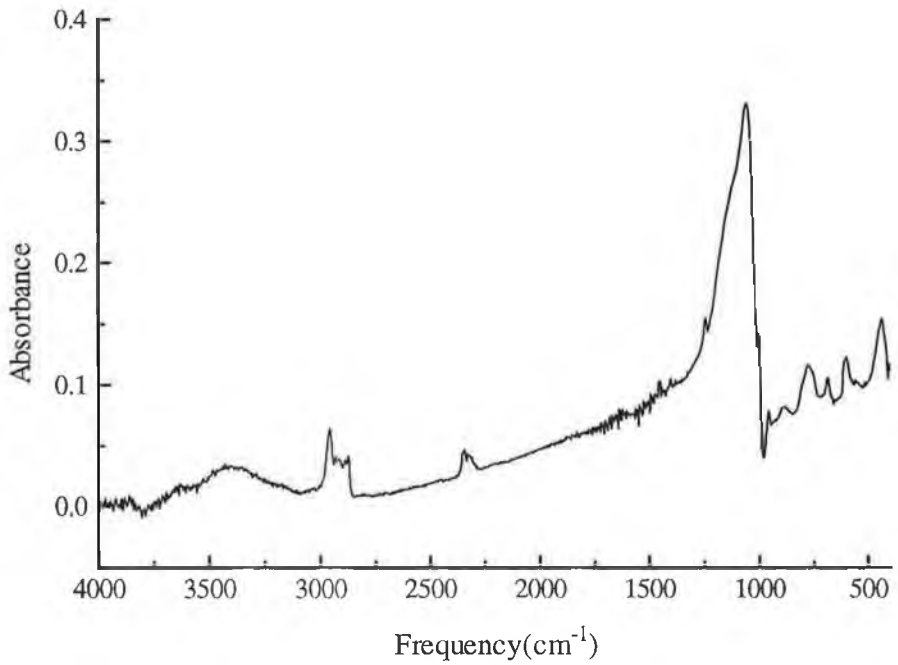

Fig 2.11 FTIR spectrum of a 1:1 ETEOS:TEOS sol-gel thin film

3400 cm^{-1} can also be seen to be significantly reduced for the ETEOS-based film. This band was completely absent for 100% ETEOS films. Thus, it was deduced that sol-gel films prepared from ETEOS would be even more hydrophobic again than those prepared from MTES, as expected from the higher aliphatic group.

To conclude, we may summarise the results as follows:

(a) A higher content of organic precursors such as MTES increases the stability and critical thickness of sol-gel thin films.

(b) The hydrophobicity of sol-gel films can be increased through the addition of an organic precursor. The hydrophobicity increases in the order

TEOS < MTES < ETEOS

(c) The total porosity of the thin films was also dependent on the sol-gel precursor. It was shown that a measure of this porosity can be derived from the FTIR spectra. The porosity appeared to increase in the order

TEOS > ETEOS > MTES

2.6 CONCLUSIONS

A detailed account of the characterisation methods for sol-gel-derived thin films prepared in our laboratory has been presented. Ellipsometry and Spectral transmittance techniques were used to determine the effect of organic precursors on the stabilisation of sol-gel thin films. The effect of these precursors on the film microstructure was characterised using FTIR spectroscopy. It was observed that the introduction of the methyl groups increased the critical thickness of sol-gel films, as well as resulting in more stable, less porous films. A detailed knowledge of the effect of organic modifiers in inorganic matrixes is critical because it allows a control of the porosity of films along with the size and shape of pores. This would be important in the preparation of coatings to be used as tailored hosts for specific reagents.

REFERENCES

1. L. Yang, S. Saavedra. **" Chemical sensing using sol-gel derived planar waveguides and indicator phases "** Anal. Chem. 67 (1995), pp. 1307-1314.

2. B.D. MacCraith. **"Enhanced evanescent wave sensors based on sol-gel derived porous glass coatings"** Sensors and Actuators B, 11 (1993), pp. 29-34.

3. F. Sheridan. **" Characterisation and optimisation of sol-gel-derived thin films for use in optical sensing"** M.Sc. Thesis (1995) Dublin City University.

4. I.M. Thomas. **"Optical coating fabrication"** Sol gel optics:Processing and parameters, Kluwer Academic Publishers (1994), pp.141-158.

5. R.M.A. Azzam, N.M. Bashara. **"Ellipsometry and polarised light"** North Holland Physics publishing (1987).

6. Rudolph Research AutoEL-III Ellipsometer, Condensed operating instructions.

7. O.S. Heavens. **"Optical properties of thin solid films"** Dover publications, New York (1965).

8. Y. Hoshino, J. D. Mackenzie. **"Viscosity and structure of Ormosils solutions"** Journal of Sol-Gel Science and Technology, 5 (1995), pp.83-92.

9. P. Innocenzi, M.O. Abdirashid, M. Gugleilmi. **"Structure and properties of sol-gel coatings from Methyltriethoxysilane and Tetraethoxysilane"** Journal of Sol-Gel Science and Technology, 3 (1994), pp.47-55.

10. A.McEvoy **"Development of an optical sol-gel-based dissolved oxygen sensor"** Ph.D. Thesis (1996) Dublin City University.

11. T.M. Butler. **"Development of evanescent wave pH sensors based on coated optical fibres"** Ph.D. Thesis (1996) Dublin City University.

12. R.M. Almeida, G.C. Pantano. **"Structural Investigation of silica gel films by infrared specrtoscopy"** Journal of Applied Physics 68 (1990) 4225

13. R.M. Almeida, H.C. Vasconcelos. **"Relationship between Infrared absorption and porosity in silica-based sol-gel films"** Proc. SPIE Vol. 2288 (1994), pp. 678-687.

CHAPTER 3

EVANESCENT WAVE CARBON DIOXIDE SENSING

3.1 INTRODUCTION

The development of sensors for the measurement of carbon dioxide concentration is of major importance for many industrial, biomedical and environmental applications. To date, gas phase CO_2 has normally been monitored via its strong absorbance in the infrared region of the electromagnetic spectrum (4.2 - 4.4μm)[1]. However in aqueous phase many interferents are known to compromise the accuracy of this technique. Furthermore, applications of IR monitors for CO_2 are limited by their price and lack of mechanical stability. As a result, much research interest has been directed towards optical sensors utilising an immobilised analyte-sensitive reagent as the key element of the sensing chemistry. This type of sensor can be small, cheap, disposable and through the incorporation of fiber optics, can be used for remote and distributed sensing.

Although a number of colorimetric CO_2 sensors have been reported[2,3], luminescence-based indicators have predominantly been employed. A detailed review of luminescence-based reagents and sensor systems for CO_2 detection is presented by Orellana et al.[4]. As highlighted in this review, the most popular fluorometric indicator, by far, for CO_2 sensing has been HPTS (Hydroxy Pyrene TriSulfonic acid - frequently referred to as Pyranine). This is mainly due to two factors (a) the excitation band of HPTS strongly overlaps the emission of commercially available blue LEDs and (b) there is a relatively large Stokes shift of 2800 cm^{-1}. In this chapter, results for a fibre optic CO_2 sensor based on the evanescent wave excitation of sol gel immobilised HPTS are presented. The working principles of the sensor, including evanescent wave theory, sensing configuration and indicator chemistry are described. Factors which affect the sensor's performance are outlined.

3.2 EVANESCENT WAVE SENSING

An evanescent field is generated whenever light is totally internally reflected at an interface. Figure 3.1 depicts a plane wave propagating in an optical fibre. For all angles of incidence greater than the critical angle θ_c represented by

$$\theta_C = Sin^{-1}\frac{n_2}{n_1} \qquad \text{eqn. 3.1}$$

light is totally internally reflected and travels along the length of the waveguide. At each reflection from the waveguiding interface the electric field amplitude does not drop to zero as might be expected, but instead extends a short distance into the lower refractive index medium. This evanescent field decays exponentially from the waveguide interface. The distance over which the field decays to 1/e or 37% of its amplitude at the interface is defined as the penetration depth[5], and is expressed as

$$d_p = \frac{\lambda}{2\pi n_2\left[\left(\frac{n_1}{n_2}\right)^2 Sin^2\theta - 1\right]^{\frac{1}{2}}} \qquad \text{eqn. 3.2}$$

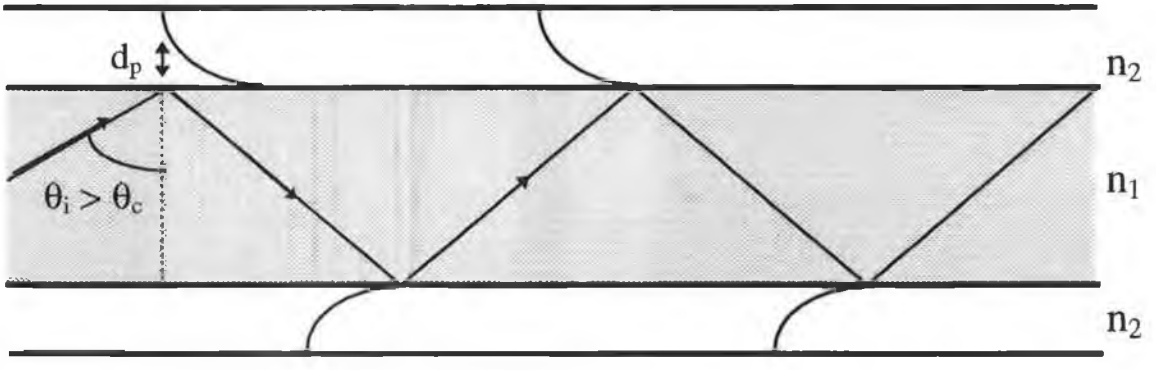

Figure 3.1 Propagation of light down an optical waveguide. The evanescent wave decays exponentially from the waveguide interface as shown.

This exponentially decaying field defines a short distance where the light may interact with molecular species in the less dense medium. If these species are absorptive, light will be coupled from the waveguide and the transmitted power will be attenuated. Alternatively, if fluorescent species are located within the evanescent field, they can be excited and the resulting fluorescence can couple back into the waveguide. If the spectral properties of these species is affected by the presence of a particular analyte, the analyte concentration can be determined by analysing the throughput of the fibre. In this context, a means of immobilising such species onto the surface of the waveguide is important.

The sol gel process described earlier is a relatively straightforward and reliable technique for the production of optical supports for indicator species[6]. The sol-gel-derived silica can be easily applied onto the fibre by dipcoating, to produce a thin microporous film around the core of the fibre. The reagent molecules are entrapped in the pores of the sol-gel matrix in a nanometer-scale cage-like structure into which smaller analyte molecules such as hydrogen ions can permeate. Furthermore, the refractive index and thickness of these films can be tailored so as to maximise the interaction between the propagating modes in the core and the indicator species. One of the main advantages of this sensing approach is that no bulk components are required in the sensing region as the interrogating light remains guided. As a result considerable sensor miniaturisation is feasible.

3.3 SENSOR PREPARATION

3.3.1 Preparation of HPTS doped sol

The HPTS doped sol was prepared as follows: 0.08g of the HPTS dye was placed in a clean vial, to which 4.08g of methanol was added. This mixture was stirred until the dye was completely dissolved. To this solution, 2g of pH4 water was added. The pH of the water was chosen as a compromise between the observed opaqueness of pH7 sol-gel-derived films and the fast gelation times of pH1 sols. The water was adjusted to the chosen pH using Hydrochloric acid. The solution was now stirred for a couple of minutes. Finally 4.22g of Tetramethoxysilane (TMOS) was added

in a dropwise manner, stirring continuously. The mixture was now stirred for 1 hour and then aged for 17 hours at room temperature. After this period, the sol produced good quality films for between 2 to 4 hours, after which the sol became too viscous for coating purposes. The sol was found to completely gel within 30 hours ageing at room temperature.

3.3.2 Sensor fibre preparation

The type of fibre used in this work was plastic clad silica (PCS) fibre of core/cladding diameter 600/760μm with a numerical aperture of 0.4. This fibre was prepared for coating with a sol-gel thin film as follows,

(i) The fibre was firstly cut into 10cm long sections using a fibre cutter. However due to the large size of the fibre, a good finish on the fibre ends was not possible by simply cleaving the fibre. As result the fibre ends had to be polished prior to their use. This was achieved using a polishing rig and two polishing plates. A steel plate was used with both 9μm and 3μm polishing solutions while a polyurethane plate was used with a 0.125μm particulate solution. The fibre ends were held in a chuck on top of the rotating polishing plates while the polishing solution was slowly added. The two larger particulate solutions removed any cracks or deformations on the fibre ends while the 0.125μm solution was used to produce a good quality finish. Each polishing step took approximately 3 hours. After the final polishing step, the fibre ends were inspected, and the above process was then repeated for the opposite ends.

(ii) After polishing, the fibres were cleaned to remove any of the polishing residue. The primary coating was then removed from ~7cm of the fibre length using a scalpel. The polymer cladding was removed using a commercially available methylene chloride-based solvent. The fibres were left in this solution for about 5 minutes and then washed in water. Each fibre was then individually cleaned with ethanol and lens tissue. The cleaned fibres were finally conditioned in de-ionised water at 73°C for 17 hours prior to coating. This was considered as having the effect of increasing the concentration of silanol (SiOH)

groups on the surface of the glass and thereby improving the adhesion of the sol-gel coating to the surface.

The optical fibres were coated with the indicator-doped sol by means of the dip coating process described in section 2.2. In this coating technique, the substrate is immersed into the sol gel solution and then withdrawn at a constant controlled speed. During withdrawal, a thin film (100nm - 1μm) becomes entrained on the substrate. Using this technique ~ 6cm of the fibre length was coated with the HPTS doped sol. An epoxy was placed on the fibre ends during coating to prevent direct excitation of the indicator dye. The coated fibres were then stored at room temperature for 3 days prior to their use.

3.3.3 Indicator Theory

Since its introduction into optical pH sensing, HPTS is the mostly widely used fluorescent pH indicator due largely to its high quantum yield, its high absorbance and excellent photostability. As a result, it has been demonstrated to be a good choice for carbon dioxide sensing. Under blue excitation (450nm), where the basic form of the dye is excited, HPTS has a pK of 6.55 and an operating range of +/- 1.5 pH units of the indicator pK[7]. The pH range can be extended by exciting the dye below 400nm, where both the acidic and basic forms of HPTS are excited with equal efficiency. A pH range of 0 to 9 has been reported by Schulman[7] by exciting HPTS in the UV region of the spectrum.

In figure 3.2 excitation and emission spectra of HPTS, dissolved in de-ionised water, recorded on a laboratory fluorimeter are shown. The dye can be seen to absorb strongly in the blue region of the spectrum with a fluorescence emission peaking at ~515nm. The excitation spectrum, which has a maximum at 420nm, closely matches the emission of blue LEDs.

The sensing mechanism of HPTS to CO_2 is as follows: CO_2 diffuses into the sol-gel film and reacts according to the following equation[7]

$$CO_2 + H_20 \Leftrightarrow H_2CO_3 \Leftrightarrow H^+ + HCO^-_3 \qquad \text{eqn. 3.4}$$

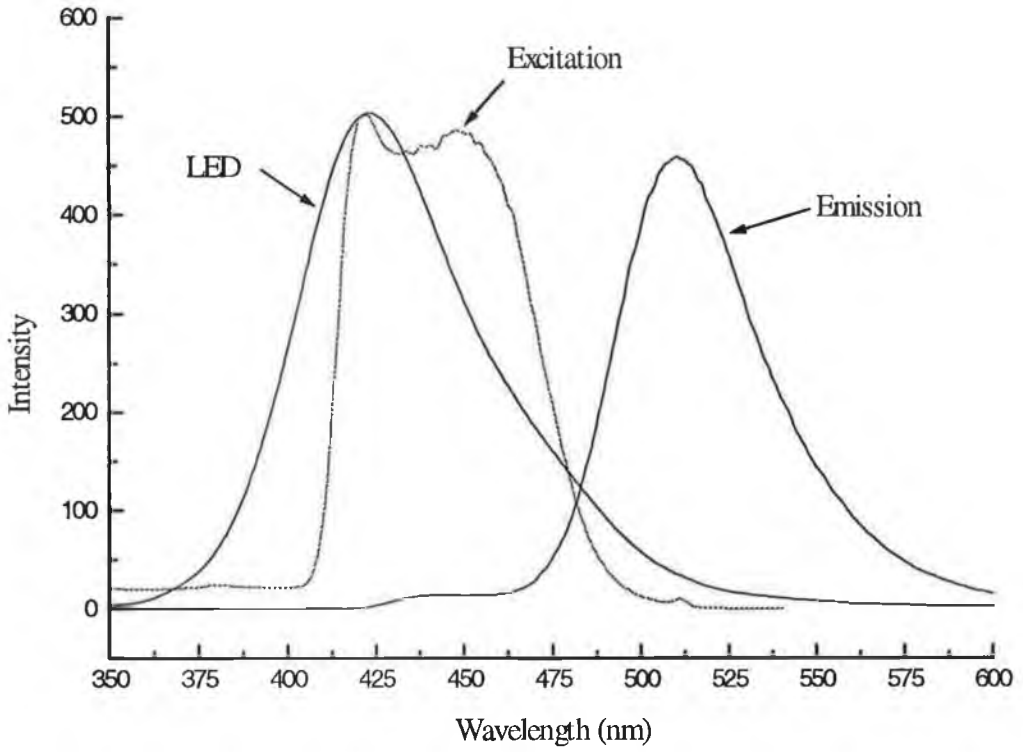

Figure 3.2 Excitation and emission spectra of 8-Hydroxy-1,3,6 pyrenetrisulfonic acid dissolved in pH 7 water. Also included is the emission spectrum of the blue LED used to excite the HPTS dye.

The increase in hydrogen ion concentration results in a decrease in the pH of the sensing layer and as a result inhibits the dissociation of the fluorescent indicator according to the following equilibrium

$$In^- + H^+ \Leftrightarrow HIn \qquad \text{eqn 3.5}$$

where In^- and HIn represent the deprotonated (base) and protonated(acid) form of HPTS, respectively. Therefore, since the deprotonated form of HPTS (In^-) is the fluorophore, the CO_2 concentration can be determined from the change in emission intensity. In effect the hydrogen ions form a non-fluorescent compound (HIn) with the fluorophore In^- .

3.4 EXPERIMENTAL SYSTEM

The experimental system for an evanescent wave carbon dioxide sensor based on a sol-gel-immobilised HPTS dye is shown in figure 3.3. The indicator dye was immobilised onto the sensing fibre as described earlier. This fibre was then placed in a sealed gas cell where the concentration of carbon dioxide was regulated using mass flow controllers. Fluorescence intensity measurements of the sol gel entrapped dye were obtained using a simple and inexpensive LED (150mCd, 420nm). Optimum launching of the LED into the sensing fibre was achieved by first polishing the LED dome down to a level close to the emitting surface. Various grades of polishing paper were then used to achieve a good quality finish on the LED surface. A convex lens (A) of 10mm focal length was then placed 10mm from the LED, resulting in a collimated beam which filled the aperture of the 0.65 NA microscope objective lens B. A bandpass filter F_1 (340nm-440nm) was used to prevent the output tail of the LED being launched into the fibre and

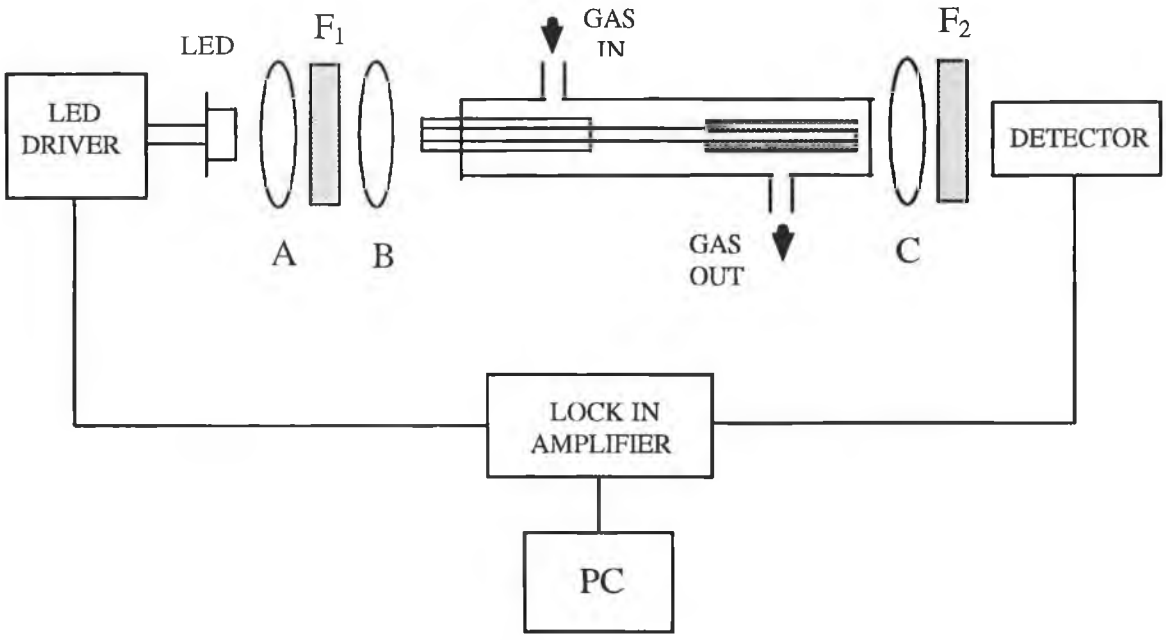

Figure 3.3 Experimental system for an evanescent wave carbon dioxide sensor

passing through the second filter F_2. The fibre was positioned using an XYZ stage and the launched intensity was maximised. The resulting fluorescence was collected from the distal end of the fibre and focused using another 10mm focal length lens onto a photomultplier tube for detection. Filter F_2 was a highpass filter with a 95% transmission above 490nm. The transmittance of the filter combination F_1 and F_2 was measured using a spectrophotometer and found to be less than 0.1%. Therefore, the only signal, that should be detected by the PMT is the fluorescence signal from the evanescently excited HPTS dye. A further increase in signal to noise ratio was achieved by pulsing the light source and employing lock-in detection techniques. This was achieved using the circuit shown in appendix 1.

3.5 SENSOR PERFORMANCE

The experimental system described in section 3.3 was set up to evaluate the sensor performance. Upon excitation with the 420nm LED, a low intensity blue/green glow was visible from the coated section of the fibre. Using mass flow controllers, varying mixtures of nitrogen and carbon dioxide gas were passed through the gas cell at a rate of 500 cm^3 /min. Upon exposure to CO_2, fluorescence quenching occurred as expected. Fluorescence intensity data obtained from the sensor are shown in figures 3.4 and 3.5. In figure 3.4 the response to alternating cycles of 100% N_2 and 100% CO_2 gas is shown. The sensor shows good repeatability with a reasonably high signal to noise ratio. It is difficult to determine the response time of the sensor simply from the graph, due to the uncertainty in the time it takes the cell to reach a particular concentration equilibrium. However t_{95}, the time taken by the sensor to reach 95 % of its final value, is certainly less than 20 seconds, while the reverse reaction ($CO_2 \rightarrow N_2$) is between 20 to 40 seconds. In figure 3.5 the sensor response to 20 % increments in CO_2 concentration is shown. The largest sensitivity to CO_2 is clearly in the range 0 to 20 % CO_2. In the 20 to 100 % range the response is approximately linear.

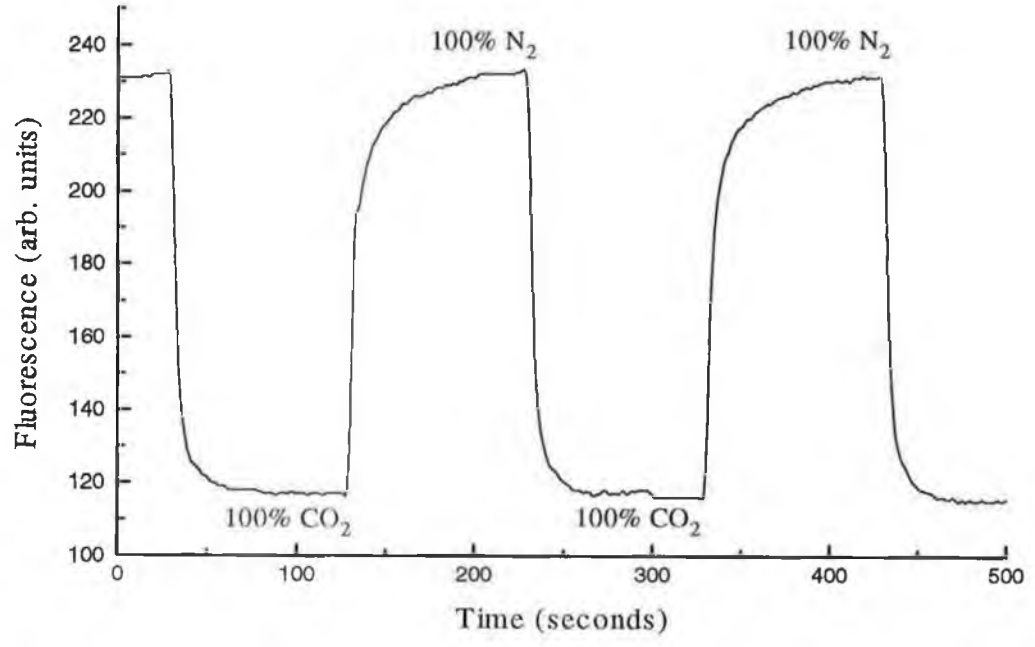

Figure 3.4 **Sensor response to repeated cycles of nitrogen and carbon dioxide gas**

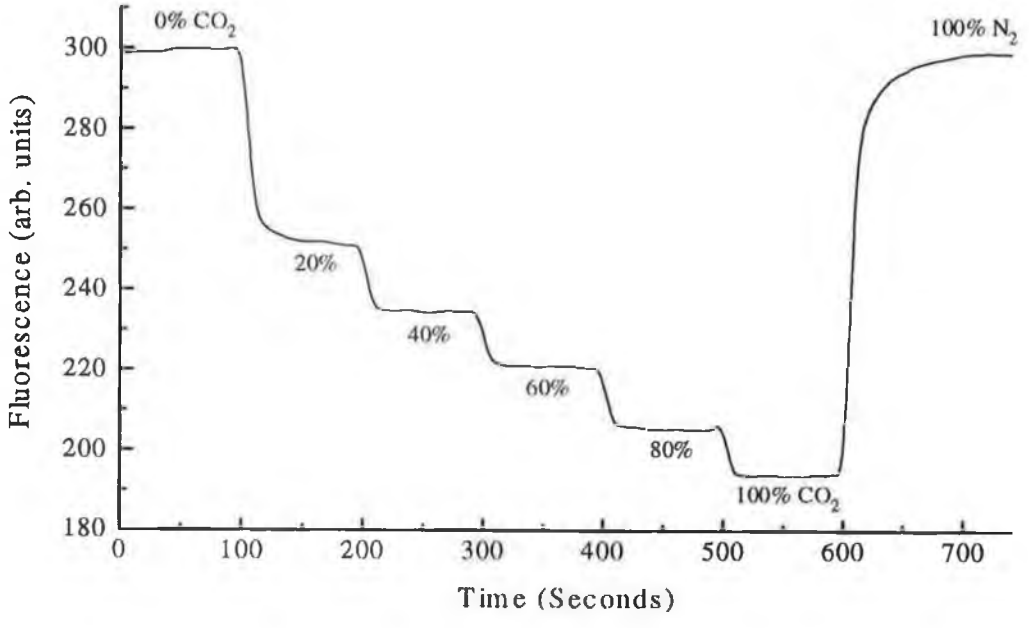

Figure 3.5 **Sensor calibration data in 20% increments from 0% to 100% carbon dioxide**

In order to determine the long term stability of the sensor, the sensing fibres were stored in air for two months and then tested again using the system described above. Over this period, the sensitivity of the sensor to CO_2 was found to have significantly decreased. To quantify the sensitivity of the sensing films to carbon dioxide, the ratio $R_{NC} = F_N / F_C$, where F_N and F_C are the fluorescence signals in nitrogen and carbon dioxide respectively, was employed as a figure of merit. For the 2 month old films the R_{NC} value was < 0.2 compared to a value of ~2 for the new films. The response time of the sensor was similarly affected, with typical response times of ~300 - 400 seconds for the 2 month old films compared to original values of 20 seconds.

This decrease in sensor performance may have been related to the change in the water concentration in the sol-gel matrix over the 2 month period. It was expected, that over this period, the water content of the sensing films decreased due to evaporation to a final level which is a function of the film environment. It is clear from eqn. 3.4 that the sensitivity to CO_2 is directly related to the water content of the sensing films. In effect, the CO_2 that diffuses into a completely de-hydrated film will not alter the pH of the film environment, and thus the sensor output would remain unaffected. It should be noted that the sensing films were aged at room temperature after coating, so the new films would be expected to have a high water content.

The sensing fibres were now placed in water for 1 hour and then tested again. In figure 3.7 the quenching response for one such fibre is shown. It should be noted that this is not the same fibre as in figures 3.5 and 3.6 so variation in sensor response might arise. Nevertheless, the change in the diffusion rate for N_2 was unexpected. The reason for this change is unknown. From the graph, however, it is clear that the sensing layer has become re-hydrated, resulting in a recovery in the sensitivity to CO_2. Therefore, to achieve a repeatable response to CO_2 , it would be necessary to either store the sensing fibres in water or re-hydrate the fibres prior to their use.

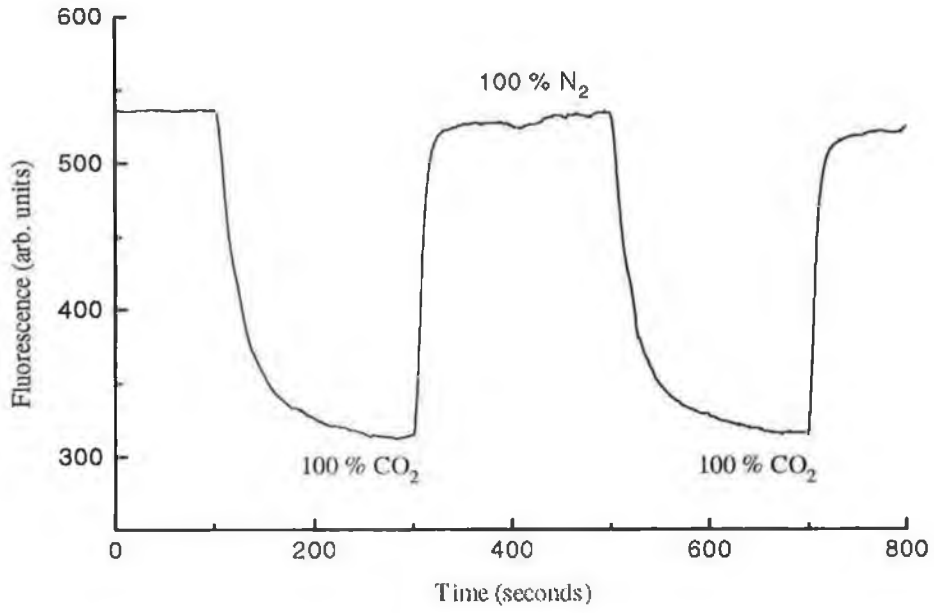

Figure 3.7 Re-hydrated (1 hour) HPTS sol gel film after storage in air for 2 months

3.5 CONCLUSIONS

In this chapter preliminary results for a fiber optic CO_2 sensor, based on the evanescent wave excitation of a sol gel immobilised fluorescent indicator, have been presented. However, from the results it is apparent that two issues need to be addressed:

(i) In gas phase measurement, the films tend to dry out, resulting in larger response times and reduced sensitivity. Thus, for gas phase measurements, a membrane which would be permeable to CO_2 but impermeable to water vapour would be necessary to maintain constant signal levels with time. Otherwise, applications of the sensor would seem to be limited to dissolved CO_2 sensing.

(ii) Sensor response is pH dependent, therefore in an aqueous environment a gas permeable hydrophobic membrane would be required to differentiate between CO_2 and pH changes.

However, despite these drawbacks, the results still are a good basis for the further development of a fiber optic CO_2 sensor.

REFERENCES

1. S. Bendamardji, Y. Alayli, S Huard. **" Capteur de CO_2 à fibres optiques par absorption moleculairé à 4.3 μm"** J. Phys. III France (1996), pp.491-503.

2. A. Mills, Q. Chang. "**Colorimetric polymer film sensors for dissolved carbon dioxide"** Sensors and Actuators B 21 (1994), pp.83-89.

3 B.H. Weigl, A. Holobar, N.V.Rodriguez, O.S. Wolfbeis. **"Chemically and mechanically resistant carbon dioxide optrode based on a covalently immobilised pH indicator"** Analytica Chimica Acta 282 (1993), pp. 335-343

4. G. Orellana, C. de Dios, M. Moreno-Bondi, M.D. Marazuela **"Intensity- and lifetime-based Luminescence optosensing of carbon dioxide"** Chemical, Biochemical and Environmental fiber sensors VII, Proc. SPIE Vol. 2508 (1995), pp 63-69.

5. B.D. MacCraith **"Enhanced evanescent wave sensors based on sol-gel derived porous glass coatings"** Sensors and Actuators B, 11 (1993), pp.29-34

6. B.D. MacCraith, C.M. McDonagh, G. O'Keeffe, A.K. McEvoy, T. Butler, F.R. Sheridan. **"Sol gel coatings for optical chemical sensors and biosensors"** Sensors and Actuators B 29 (1995), pp.51-57.

7. S.G. Schulman, S. Chen, F. Bai, M.J.P. Leiner, L. Weis, O.S. Wolfbeis. **"Dependence of the fluorescence of immobilised 1-hydroxypyrene-3-6-8-trisulphonate on solution pH: extension of the range of applicability of a pH fluorosensor"** Analytica Chimica Acta 304 (1995), pp.165-170

8. X. He, G. Rechnitz **"Linear response function for fluorescence-based fiber-optic CO_2 sensors"** Analytical Chemistry (1995) 67, 2264-2268

CHAPTER 4

POINT SENSING

4.1 INTRODUCTION

For many applications, especially in biological sensing, the design of miniature sensors that permit in situ on-line measurements is of major interest. Optical fibres would appear to be ideal for this application. Their inherent characteristics, as discussed in section 1.2 along with their extremely small size, determined by the fibre diameter, permits invasive measurements such as the analysis of blood arteries and cells. In this regard, much research has been directed towards point sensing using the tip of optical fibres. Much of this work has concentrated on attaching a membrane or capillary, containing the specific reagent, to the fibre end[1,2]. However the commercial exploitation of this technique have been limited by a number of factors: (i) the cumbersome task of assembling the sensor head, (ii) the small signal return due to the small interaction area with the fibre end, and (iii) the long response time, due to slow diffusion of the analyte through the membrane wall. Recently, micron - size[3] and even submicrometer[4] optical fibre sensors have been fabricated for pH and oxygen sensing. However due to difficulties in capturing the fluorescence signal from the end of the sensing fibre, both these approaches used a microscope objective at the distal end of the fibre to detect the fluorescent signal. A more attractive approach would employ the same fibre to both transmit the excitation light and collect the resulting fluorescence. In such a way only the proximal end of the fibre requires coupling optics, thus facilitating remote sensing applications.

In this chapter, the use of standard telecom fibre with a core size of 50μm as a sensor support is discussed. Analyte-sensitive reagents are attached to the fibre via a novel configuration at the fibre tip. This configuration was achieved by etching a cavity into the tip of the fibre, which was then filled with indicator doped sol-gel-derived silica. Results for oxygen and pH single point sensing using fluorescence based indicators are

presented. In addition, preliminary results for single point ammonia sensing using an absorption-based indicator are presented. Finally, problems associated with the absorption approach are discussed.

4.2 SENSOR TIP FABRICATION

4.2.1 Preparation of indicator doped sol

The method of preparation for the indicator doped sol is as follows: 2.075g of water is placed in a clean vial along with 4.15g of ethanol in which the dye is dissolved. The pH of the water was adjusted to pH 1 using hydrochloric acid. These are stirred until the dye is completely dissolved. 6g of methyltriethoxysilane (MTES) is then added dropwise to the solution. The mixture is then stirred for an hour prior to coating. In contrast with Tetraethoxysilane (TEOS)-based sols, ageing for a period of time at 73°C was not necessary. This recipe used was preferred over a TEOS-based sol-gel recipe, as films from the former recipe have proven to have better thickness stability over time (section 2.4). It was expected that the MTES derived silica would shrink to a lesser degree while packed in the fibre cavity and would therefore be expected to be more securely bound to the fibre tip.

4.2.2 Fibre preparation and sol-gel immobilisation

The technique employed for immobilising chemical reagents onto telecom fibre is presented here. The fibre normally used is 50/125 graded index tele-communications fibre. The polymer coating is removed from the fibre using a methylene chloride stripper. The fibre is then cleaved using a commercial fibre cleaver (Fujikura CT-07) and inserted into hydrofluoric (HF) acid. Telecommunications fibre has a parabolic refractive index profile, the purpose of which is to minimise pulse spreading in high speed communications systems. This profile is achieved by incorporating dopants

such as germania into the silica, during fibre preparation. The index of refraction is greatest in the centre and decreases approaching the cladding. Since the etching rate increases with dopant concentration, a parabolic shaped cavity is etched into the tip of the fibre representative of its refractive index profile[5,6]. The result of this process is shown in figure 4.1, where a standard refractive index profile of a graded index fibre together with a magnified image of an etched fibre tip is presented. For 40% HF acid an etching rate of approximately 10 microns/min was observed. After etching, the fibre is conditioned in de-ionised water for 24 hours in order to improve the adhesion of the sol-gel derived silica to the cavity walls. The fibre cavity is then packed with sol-gel-derived silica, doped with an analyte sensitive dye, by means of successive cycles of dipping and curing. This produces a micro-porous silica matrix which entraps the dye, while allowing access by the analyte[7]. Moreover, the sol-gel support matrix is intrinsically bound to the fibre core in a manner which yields a mechanically stable sensor tip which is not damaged easily. In figure 4.2, a magnified image (head-on) of a cavity packed with a sol-gel matrix doped with a ruthenium complex is presented. In figure 4.3, a side-on image, taken through a red filter,

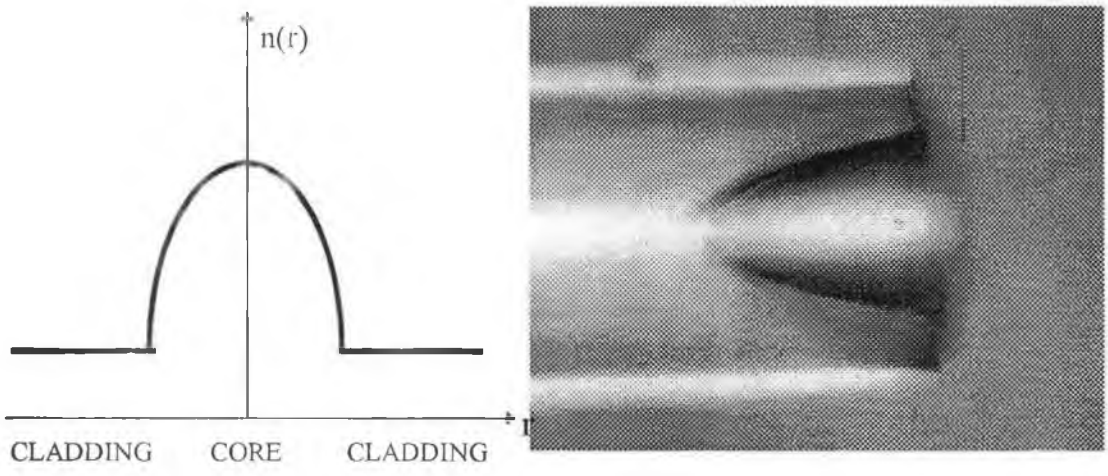

Figure 4.1 Refractive index profile and HF etched cavity of a graded index telecommunications fibre

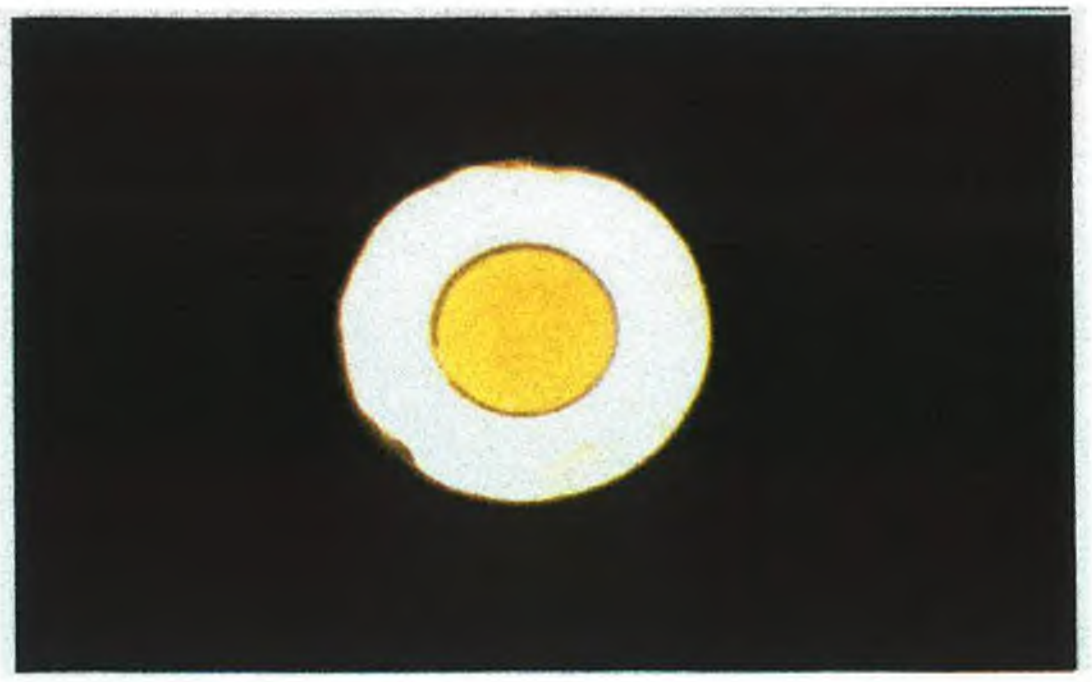

Figure 4.2 Front face magnified image of a ruthenium doped sol-gel packed fibre tip cavity

Figure 4.3 Side view magnified image of a ruthenium doped sol-gel packed fibre tip cavity

of the packed cavity, under blue excitation is shown. It can be seen from both images how effectively the sol-gel-derived silica is packed into the etched fibre tip cavity.

4.3 SENSOR TIP EVALUATION

4.3.1 Fluorescence based indicators

The cavity sensor configuration described was initially evaluated as a single point oxygen sensor using a ruthenium complex (ruthenium tris diphenyl phenanthroline) as the sensing reagent. This complex was chosen for this work as it exhibits high oxygen sensitivity due to its long unquenched lifetime τ_0 ($\approx$ 6μs). Furthermore it absorbs strongly in the blue region of the spectrum while its oxygen dependent emission is at wavelengths > 600nm. Thus, due to this large Stokes shift, the detection signals for sensor applications are easily distinguished. The experimental system used to evaluate the sensor is shown in figure 4.4. The 488nm line (50mW) from an air-cooled Argon ion laser was used to excite the ruthenium complex molecules entrapped in the sol-gel-packed cavity. The resulting fluorescence was then detected at the proximal end of the fibre, via a beamsplitter (1: 99) and longpass filter, using a photodiode detector. The beam splitting ratio was selected in order to (i) reduce the excitation intensity and thus avoid the effects of photobleaching, and (ii) to capture a large percentage of the low intensity fluorescent signal. An optical chopper and Lock-in amplifier were used to distinguish the fluorescent signal from external light fluctuations, and thus increase the signal to noise ratio. Using mass flow controllers, cycles of nitrogen and oxygen gas were passed at a rate of 500cm^3/min through the gas cell containing the fibre tip sensor. In 100% N_2 a bright orange/red glow was seen from the fibre tip. Upon exposure to O_2, fluorescence quenching occurred as expected. A typical response curve for a fibre tip oxygen sensor is shown in figure 4.5. The plot shows a high signal to noise value with good repeatability. The response time of the sensor, as would be expected, was largely dependent on the size of the cavity, due to diffusion effects. For a cavity depth of 100μm,

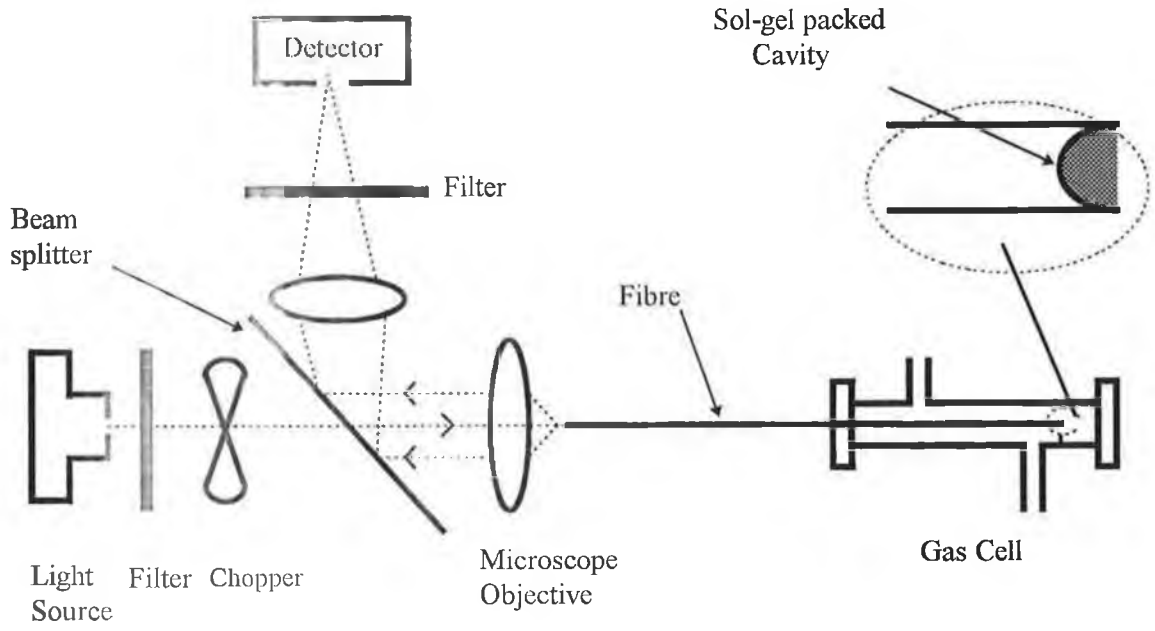

Figure 4.4 **Schematic of the instrumental set-up used for obtaining fluorescence intensity measurements from the fibre tip cavity.**

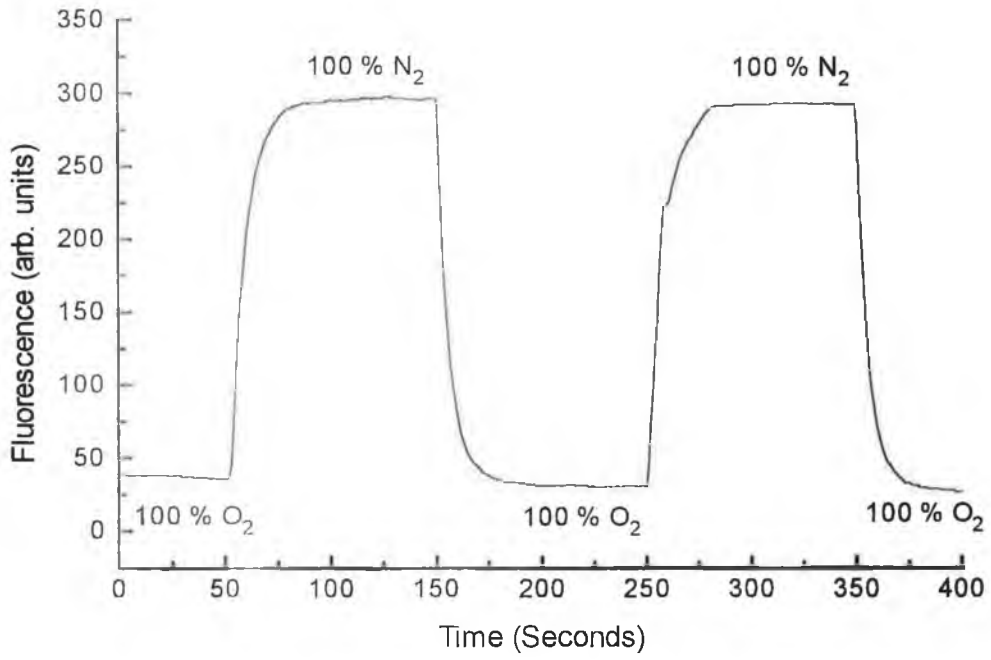

Figure 4.5 **Typical Oxygen response curve of a cavity immobilised ruthenium complex**

response times of 5 to 20 seconds were typical. This compares to 3.1 seconds for an evanescent wave fiber optic oxygen sensor using the same sensing chemistry[7].

Further evaluation was carried out using a fluorescent pH-sensitive indicator dye which was entrapped in the sol gel cavity as before. The dye used, fluorescein, is similarly excited in the blue region of the spectrum while its fluorescence is modulated by the concentration of H^+ ions. This modulation occurs via a shift in the absorption spectrum with pH. As the pH is reduced, the absorption spectrum of fluorescein shifts to longer wavelengths thereby resulting in a corresponding decrease in the emission intensity. This change is most sensitive over the pH range 3 to 6.5 pH units. In figure 4.6 the fluorescence intensity recorded as a function of 2 pH levels is shown. An argon-ion laser was again used as the excitation source. The sensor response time is longer than that for the oxygen sensor, but is still considerably less than 60 seconds.

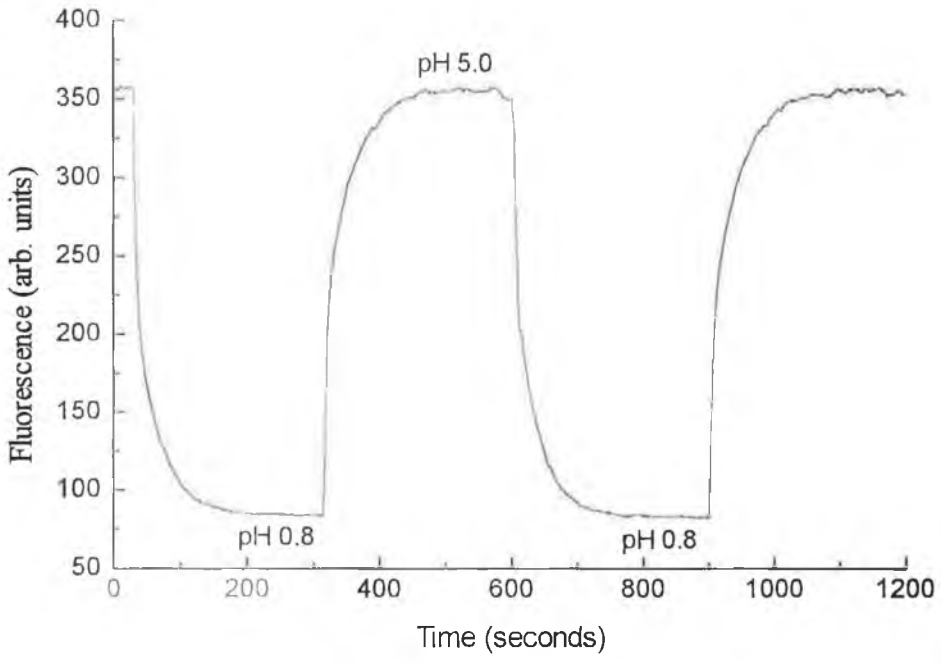

Figure 4.6 Typical response curve to pH for a cavity immobilised fluorescein dye

4.3.2 Absorption based indicators

In the previous section, the feasibility of immobilising fluorescent indicators onto the tip of an optical fibre was investigated. However a feature of currently available fluorescent indicator dyes is that their absorption bands predominantly lie in the blue region of the spectrum. This is unfortunate, since the lowest priced semiconductor light sources are available in the near infrared (NIR) spectral region. Similarly, low-priced silicon photo-detectors have much greater responsivity in this region of the spectrum. Furthermore, with remote or distributed sensing in mind, most optical fibres are silica based and thus have a minimum attenuation in the near infrared (NIR). Efforts at immobilising a NIR dye onto the tip of an optical fibre will be discussed later. It was necessary to investigate initially whether this sensing technique could be extended to absorption-based indicators. To verify this, oxazine 750 perchlorate, whose absorbance is ammonia dependent, was chosen[9]. In figure 4.7 results are presented for the spectra of this dye immobilised in a sol gel thin film, before and after exposure to ammonia vapour. As can be seen from the spectra, the absorption maxima of the dye coincides very closely with 670nm laser diodes. Laser diodes offer a number of operational advantages over Lasers as excitation sources

(i) The output can be electronically modulated, thereby eliminating the need for moving parts

(ii) They are inexpensive, due to mass production

(iii) They are small in size and have low power consumption, thus facilitating a portable system

The experimental configuration shown in figure 4.8 was set up using a pigtailed 20mW 670nm laser diode as the light source. A Levell function generator was used to modulate the laser diode output at 1kHz to facilitate lock-in detection. A 50/50 fibre optic coupler replaced the beamsplitter used in the fluorescence work while a Hamamatsu photomultiplier was used to detect the reflected light from the sensing fibre. Further

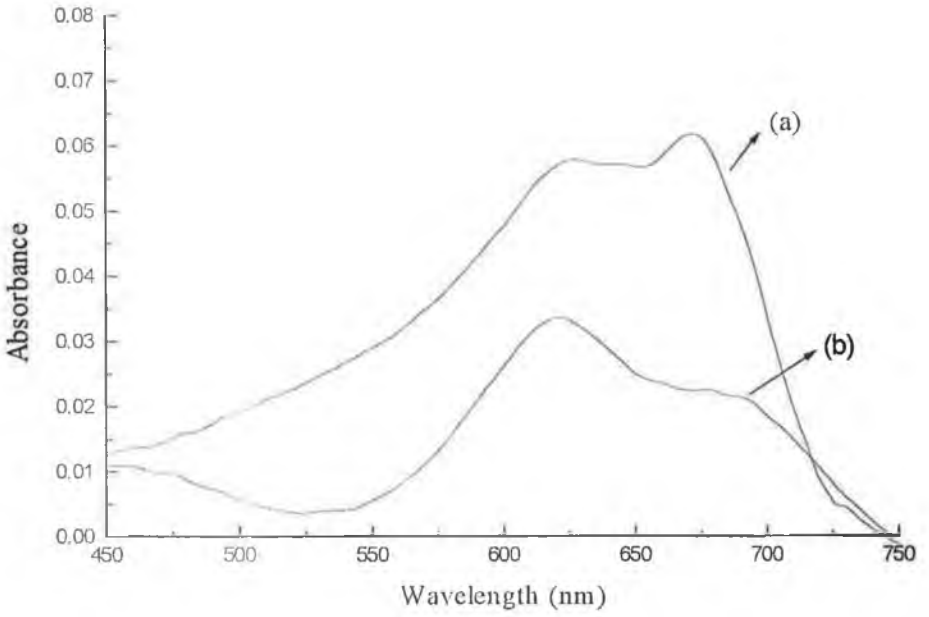

Figure 4.7 Absorption spectra of sol gel immobilised Oxazine 750 perchlorate dye (a) in air, (b) after exposure to NH_3 vapour for 10 minutes

simplification can easily be achieved by replacing the signal generator and lock-in amplifier by simple pulsing and lockin circuitry. The indicator dye was immobilised onto the tip of the sensing fibre as described earlier. In this configuration, however, steps must be taken, to enhance the return signal from the fibre tip. Otherwise only a weak reflectance signal is detected. In this regard, two approaches were examined: (i) covering the end of the fibre cavity with an analyte-permeable reflective polymer coating, or (ii) coating the fibre tip with an additional high refractive index layer. The second approach which increased the reflectance by as much as 50% was easier to configure. This approach was used in obtaining the data presented in figure 4.9. Here the real time response of the sensor when exposed alternately to environments of air and NH_3 vapour is presented. The t_{90} response time when switching from air to NH_3 vapour is approximately 2 minutes

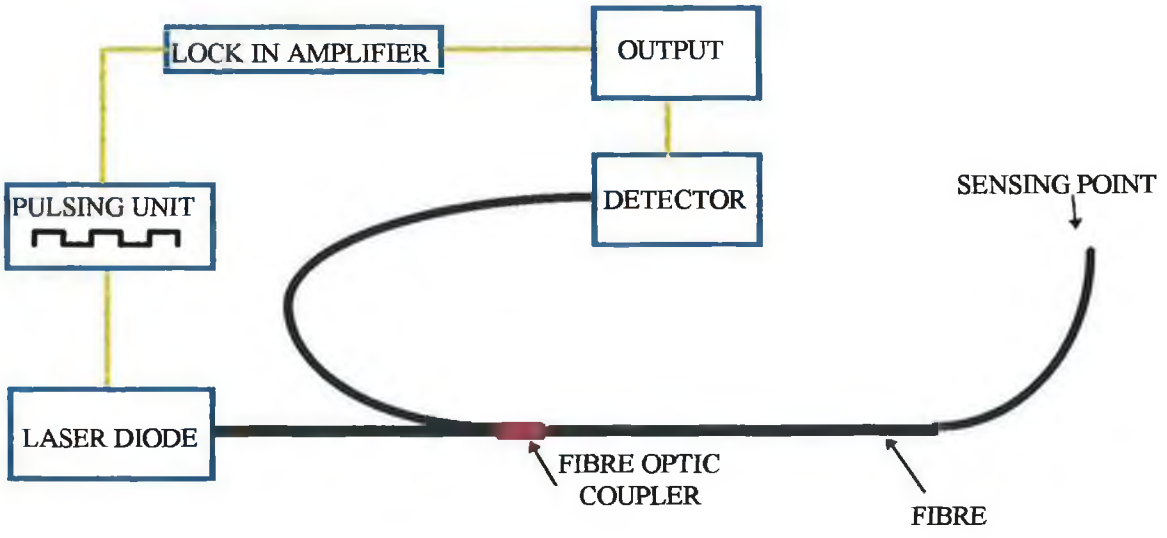

Figure 4.8 Experimental configuration for a single point ammonia vapour sensor

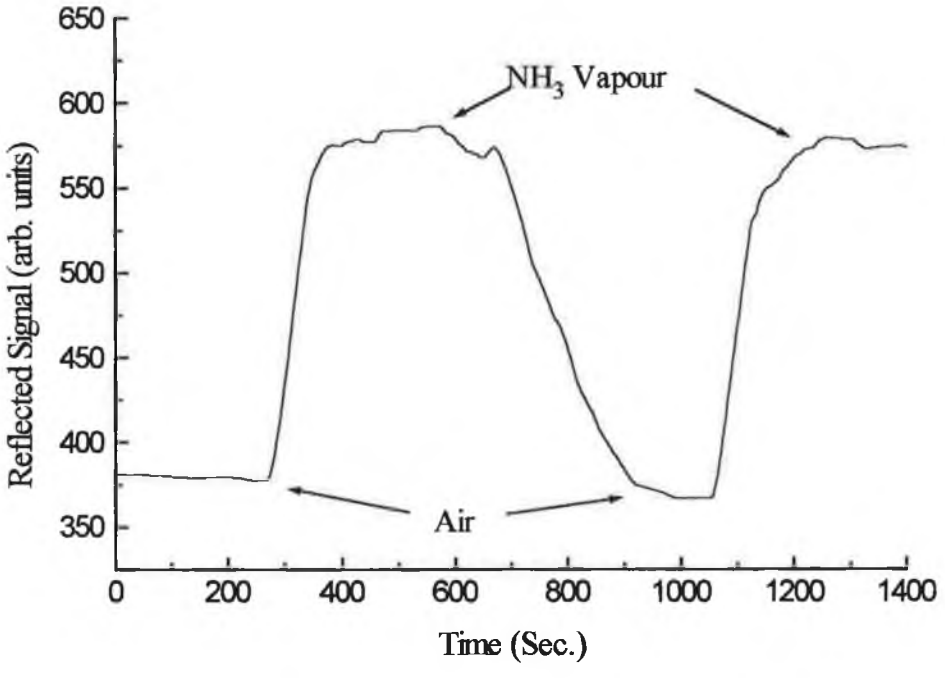

Figure 4.9 Absorption response from fibre tip cavity of sol gel entrapped oxazine dye in repeated cycles of air and Ammonia vapour

3. J. Samuel, A. Strinkovski, S. Shalom, K. Lieberman, M. Ottolenghi, D. Avnir, A. Lewis "**Miniaturization of organically doped sol gel materials: a microns - size fluorescent pH sensor**" Materials Letters 21(1994), pp.430-434.

4. Z. Rosenzweig, R. Kopelman. **"Development of a submicrometer optical fiber oxygen sensor"** Anal. Chem. 67, (1995), pp.2650-2654.

5. Q. Zhong, D. Inniss **"Characterisation of the lightguiding structure of optical fibres by atomic force microscopy"** Journal of lightwave technology, Vol. 12, No.9, (1994), pp.1517-1523.

6. Personal Communications with Dr. Brian Lawless, School of Physical Sciences, Dublin City University.

7. B.D. MacCraith, C.M. McDonagh, G. O'Keeffe, A.K. McEvoy, T. Butler, F.R. Sheridan. **"Sol gel coatings for optical chemical sensors and biosensors"** Sensors and Actuators B 29 (1995), pp.51-57.

8. B.D. MacCraith, V. Ruddy, C. Potter. "**Optical Waveguide sensor using evanescent wave excitation of fluorescent dye in sol-gel glass**" Electronics Letters Vol. 27 No. 14 (1991), pp.1247-1248.

9. L.L. Blyer, JR., R. A. Lieberman, L.G. Cohen, J.A. Ferrara, J.B. Macchesney. **"Optical fiber chemical sensors utilising dye - doped silicone polymer claddings"** Polymer Engineering and Science Vol.29, No. 17 (1989) pp.56-63.

10. Bambot, G Rao, M. Romuald, G.M. Carter, J. Sipior, E. Terpatchnig, J. Lakowicz . **"Sensing oxygen through skin using a red diode laser and fluorescence lifetimes"** Biosensors and Bioelectronics Vol. 10, No. 6/7 (1995), pp.643-652.

CHAPTER 5

QUASI-DISTRIBUTED FIBRE-OPTIC CHEMICAL SENSING

5.1 INTRODUCTION

Fibre optic chemical sensing utilising evanescent wave interactions with a doped polymer or sol gel coating has been an active research topic for a number of years[1,2]. The potential of fibre optics, however, for fully distributed or quasi - distributed multipoint sensing has not been exploited to a great extent. At present most reports of distributed sensing describe systems using large core polymer clad silica (PCS) fibre with the analyte-sensitive dye immobilised in the cladding or in a side coating. Evanescent wave interactions between the guided light and the coating/cladding provide the sensor modulation.

This technique has been used by Klimcak et al.[3] for the detection of rocket fuel propellant vapours (hydrazine and nitrogen tetroxide). In this work, a section of cladding from a 200 micron core PCS fibre was removed and replaced with a sol-gel coating doped with phosphomolybdic acid (PMA). PMA is a bright yellow oxidising agent that reacts with the rocket fuel vapours to form molybdenum oxides and hydroxides that absorb strongly in the deep red spectral region. The end of the fibre was then coated with a reflective element to return light for detection. A number of these sensing fibres were then coupled onto a fibre optic network similar as shown in figure 5.1. A pulsed 10mW 680nm laser diode was employed as the light source. The change in intensity of reflected light from each of the sensing regions was then monitored using Optical Time Domain Reflectometry while under exposure to the analytes under investigation. A modification on this approach was developed by Kharaz & Jones[4] for relative humidity measurements. In this work, a high refractive index Cobalt Chloride - gelatin film was coated along

facilitating sensing over several kilometres if necessary. Furthermore, one can exploit the proven components and associated instrumentation of the mature fibre optic telecommunications technology. In particular, connectors, couplers, cleavers, fusion splicers and OTDRs are routinely available and well established.

In this chapter, the development of a quasi-distributed sensing system employing telecom grade optical fibre is presented. The technique was enabled by the novel immobilisation technique based on fibre etching and sol-gel technology described in the previous chapter.

5.2 OPTICAL TIME DOMAIN REFLECTOMETRY

Since the late 1960's, due to advances in the quality of optical fibre material and design, the attenuation of optical fibres has decreased from over 1000dB/km to around 0.2 - 1 dB/km today. As a result, repeaterless optical communication links of longer than 50km are now an achievable reality. An offshoot of this increase in fibre lengths is the greater difficulty in locating breaks or imperfections in the fibre. This necessity has spurred the development of Optical Time Domain Relfectometers (O.T.D.R.) as essential tools in fiber optic testing applications.

An OTDR is fundamentally an optical radar. It sends out a signal and detects the "echo" signal. The basis of the OTDR technique is shown in figure 5.2. Short duration pulses (1ns-100ns) are periodically launched into the fibre under investigation by means of an optical directional coupler. Since the injected light pulse undergoes Rayleigh scattering whilst travelling down the core, some of the scattered light will travel back towards the source. The properties of the optical fibre are then determined by analysing the amplitude and temporal characteristics of this back-scattered light. The backscattered power for a graded index fibre as a function of time $P_{Ra}(t)$ may be obtained from the following equation,[5]

$$P_{Ra}(t) = \frac{P_i \gamma_R W_0 v_g NA}{12 n_i^2} \exp\left(-\gamma v_g t\right) \qquad \text{eqn. 5.1}$$

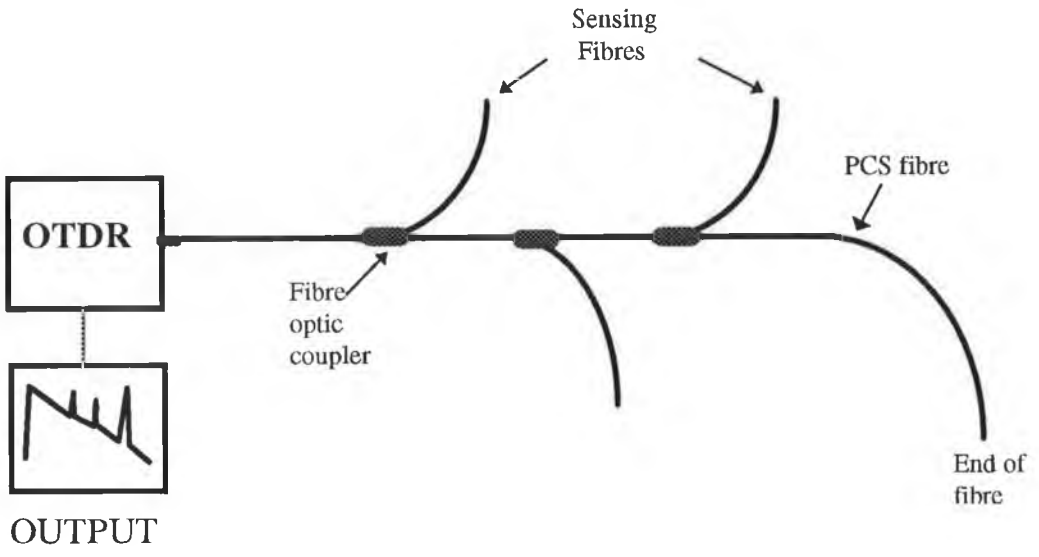

Figure 5.1 Quasi- distributed fibre optic sensor network using an OTDR-based system

sections of a 200 micron core fibre. In this case, since the refractive index of the film is slightly higher than that of the fibre core, light in the optical fibre travels through the film and interacts with the cobalt chloride molecules. As the external humidity varies so does the light absorption in the sensitive wavelength region. As in the previous sensing approach, an optical time domain reflectometer technique was used to discriminate between the various sensing regions. This approach would seem to be limited to short lengths of fibre, due to the high losses that would be incurred in replacing the fibre cladding with the high refractive index coating.

These approaches suffer from a number of drawbacks which have restricted their commercial exploitation. First, the type of fibre used is relatively expensive and there is considerable effort involved in preparing the sensing regions. In addition there are difficulties associated with cleaving and splicing such fibres. Finally, components such as directional couplers and connectors are not as well developed or as routinely available for these fibres as would be the case for standard telecom fibres.

With respect to these limitations there are clear advantages in using telecom fibre as the sensor support. These include the low attenuation and low cost of the fibre thereby

where P_i is the optical power launched into the fibre, γ_R is the Rayleigh scattering coefficient, W_0 is the input optical pulse width, v_g is the group velocity in the fibre, NA is the fibre numerical aperture, n_i is the fibre core refractive index and γ is the attenuation coefficient per unit length of the fibre. Therefore, a graded index fibre of numerical aperture of 0.2 , core refractive index 1.5 and a Rayleigh scattering coefficient of $0.7km^{-1}$, the backscattered optical power from the fibre input, for light pulses of 50ns duration, would be 47.9dB down on the forward optical power.

A typical output from an OTDR is shown in figure 5.3. Here, the log of the Rayleigh backscattered power as a function of time (and thus distance along the fibre) is shown. The initial pulse is caused by reflection and backscatter from the fibre input. The downward slope in the trace is caused by the distributed Rayleigh scattering from the input pulse as it travels along the fibre. Also shown in the plot are pulses corresponding to reflections from a mechanical splice and the fibre end, as well as discontinuities due to excess losses at fibre splices.

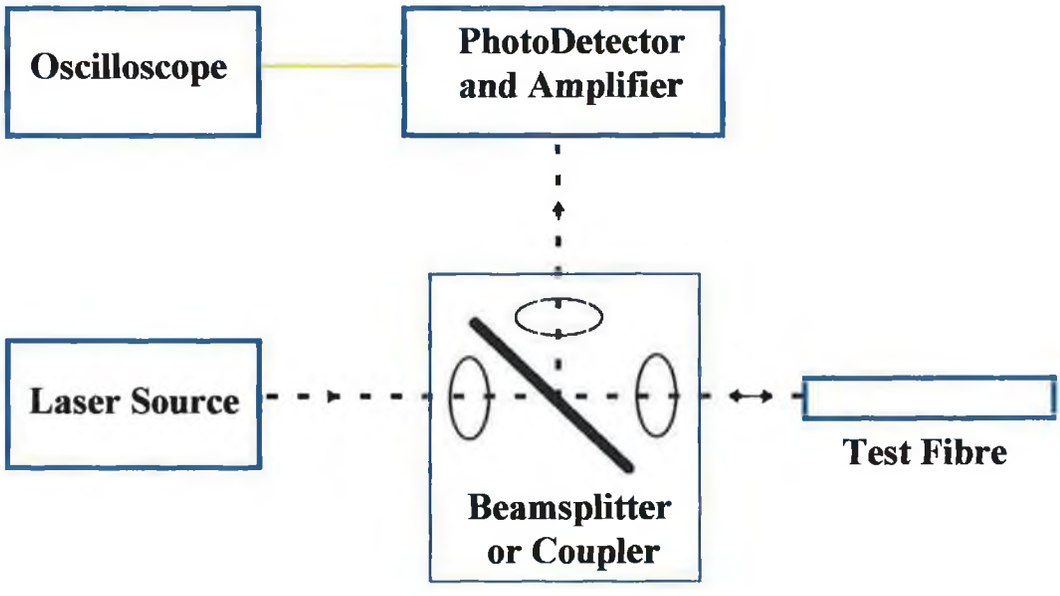

Figure 5.2 Operating principle of an optical time domain reflectometer

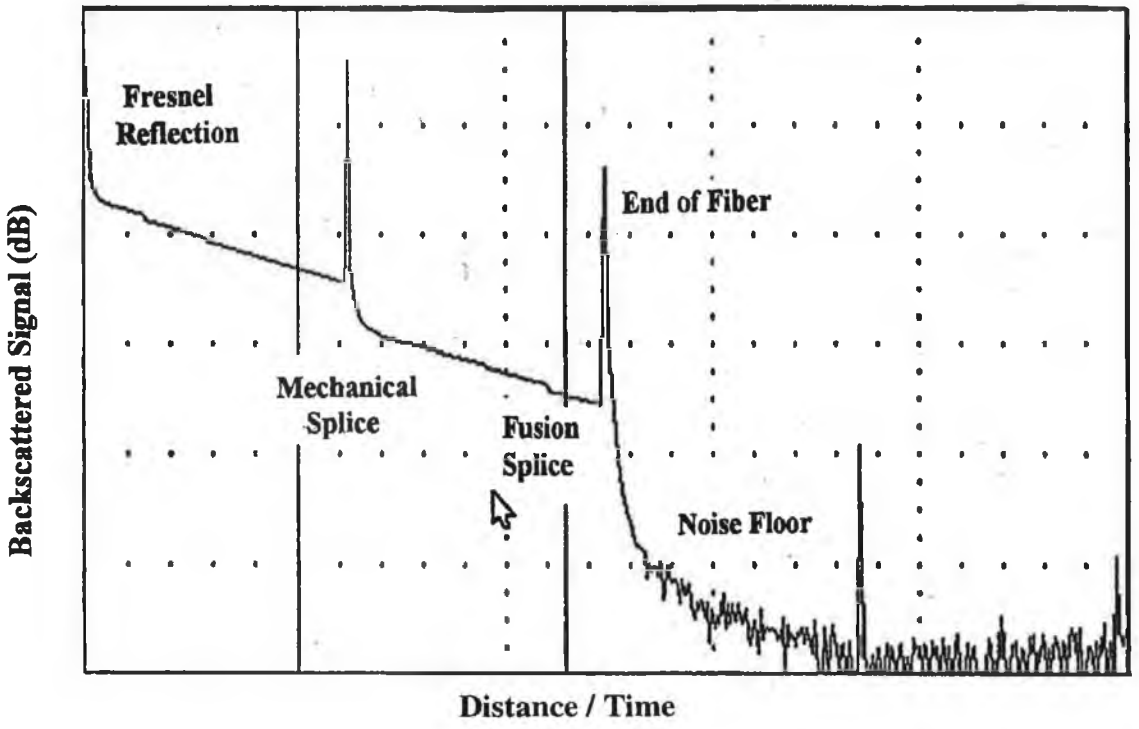

Figure 5.3 Standard trace from an optical time domain reflectometer

Such a plot yields the attenuation per unit length of the fibre by simply computing the slope of the curve over the length required. Also, the insertion losses of splices can be obtained from the power drop at the respective splice positions while the location of discontinuities in the return signal, can be determined approximately using the following equation

$$D = \frac{(c \times t)}{2n} \qquad \text{eqn. 5.2}$$

where c = speed of light in vacuum

t = return pulse time delay

n = index of refraction of fibre under test.

Therefore, by measuring the time delay (t) between the excitation pulse scattered from the fibre front and the subsequent scattered signals, the location of any number of features may be determined. When this technique is combined with immobilised chemical reagents it should be possible to determine the concentration and spatial distribution of an analyte along the length of a single fibre or at discrete sensing points (quasi distributed sensing).

The main parameters of interest concerning OTDR systems are (i) the spatial resolution, (ii) the backscattered signal resolution and (iii) the dead zone.

(i) The spatial resolution (i.e. the minimum distance between two features which can be resolved) of OTDR systems is dependent on a combination of the width of the light pulse and the response time of the detection system. Detectors with sub-nanosecond response times are now commercially available while pulse widths of around 5ns are easily achievable, leading to spatial resolutions of around 1m.

(ii) The signal resolution of OTDR systems is dependent on the minimum detectable power P_{min} of the systems detector. It can be shown that

$$P_{\min} \propto NEP\left[\frac{1}{2N\Delta t}\right]^{\frac{1}{2}} \qquad \text{eqn 5.3}$$

where NEP is the noise equivalent power, N is the number of averages carried out of the backscattered signal, and Δt is the light pulse duration. Due to the small backscattered signal (typically 45-60dB down on the forward power) a large number of averages is generally necessary. The resolution of the system could also be increased by using higher laser pulse powers. Commercial OTDR systems typically emit peak power pulses of between 20-500mW.

(iii) The dead zone of an OTDR is the region where the electronics are saturated with the reflected and backscattered signal from the fibre input. The dead zone thus determines the minimum resolvable distance to the first feature in the fibre. A dead zone distance of 5m is typical for commercial OTDR systems.

5.3 FLUORESCENCE VS. ABSORPTION-BASED INDICATORS

In the previous chapter, both fluorescence and absorption-based indicators were used as reagents in point sensors. In the sensing configuration employed, fluorescence indicators proved to be more attractive, because, in general, they gave a larger return signal than absorption-based indicators. However, for a quasi-distributed system, one must consider the effect of fluorescence decay time on the achievable spatial resolution. For example, the ruthenium complex referred to in the previous chapter has a fluorescence decay time of ca. 5μs in nitrogen. Taking account of the speed of light in the optical fibre, and the time delay between the excitation of the various sensor points, this corresponds to approximately 500m spatial extent! In other words, to discriminate between two successive sensor points, they would have to be separated by at least 500m of fibre. Thus, long lived species such as the ruthenium complex would not be the ideal choice of indicator in a quasi-distributed system. In this regard, some consideration was given to using an oxygen sensitive osmium complex which has the dual advantage of deep red excitation and shorter fluorescence decay times (typically <500ns). Fluorescence quenching is described by the Stern-Volmer equation,[6]

$$I_0/I = 1+k\tau_0[O_2] \qquad \text{eqn. 5.4}$$

where I_0 = Fluorescence quenching in absence of oxygen

I = Quenched intensity in presence of oxygen

k = Bimolecular quenching coefficient

τ_0 = Unquenched lifetime of sensing complex

Therefore, sensors based on the quenching of a fluorophore have lower sensitivity the shorter the fluorescence decay time of the fluorophore. As a result osmium complexes exhibit much lower fluorescence intensities than equivalent ruthenium complexes. Therefore a trade-off exists between spatial resolution and sensitivity in fluorescence quenching systems. However this problem does not arise for absorption based systems. The spatial resolution of these systems would only be limited by the system electronics. Thus, despite the poorer sensitivity of absorption based indicators, it was concluded that

this approach was the more attractive option for a quasi-distributed system. The viability of this conclusion will be examined in the following sections.

5.4 DISTRIBUTED SENSING SYSTEMS

Two approaches were investigated in order to develop a quasi-distributed chemical sensor system.

1. The use of commercially available OTDR systems which operate at telecom wavelengths (850nm,1300nm,1550nm). This would necessitate the selection of an appropriate indicator dye which absorbs in the appropriate spectral region.
2. The design and construction of an OTDR system at a wavelength compatible with a particular indicator dye, which can be interrogated in the visible region using laser diodes and fast electronic pulsing / detection circuits.

5.4.1 Commercial 850nm OTDR

An OTDR (EXFO-FCS-100)[7] operating at 850nm was obtained from EXFO Electro-Optical Engineering, Quebec, Canada. The OTDR is integrated within a PC compatible card with variable pulse width settings of 5 to 275ns and an output power of 20mW. The signal resolution was found to be in the order of 0.01dB, which corresponds to a typical splice loss . The dead zone of the OTDR was 5m while its spatial resolution was 1m at the 5ns pulse setting. The test fibre was connected to the OTDR by means of a ST coupled fibre which was fusion spliced onto the test fibre. The incident light was then tapped off into 3 sensing fibres in a configuration similar to that shown in figure 5.1 using fibre optic couplers. The coupling ratios were chosen so that each sensor point was illuminated with approximately 15% of the launched intensity. These sensing fibres were prepared as described in section 4.2. Approximately 4% of the incident light at each sensor point was expected to be returned for measurement (fresnel reflection from a glass-air interface). However as was described earlier, this signal can be enhanced by using a reflective element at the sensing points.

5.4.2 Design and construction of a 670nm OTDR

As mentioned earlier, one of the most fundamental parameters in designing an OTDR system is the spatial resolution of the device. This is governed by a combination of the laser pulse width and the detector response time. As a result, to achieve the goal of high spatial resolution and high sensitivity, circuit design for both the pulsing and detection systems is critical for the successful implementation of an OTDR device.

In Appendix B the circuit diagram designed to modulate the OTDR laser diode is shown. The circuit was designed to output a TTL signal of 50ns duration with varying duty cycle. In this work, a duty cycle of 14 was chosen, i.e. the 50ns pulse was repeated every 700ns. The laser diode used, purchased from Laser 2000 (UK), had an output CW power of approximately 10mW at 670nm. This signal could be modulated to achieve 10mW pulses of 50ns pulse duration by means of an external TTL input from the laser diode pulsing unit. This corresponds to a spatial resolution of 10 metres. In

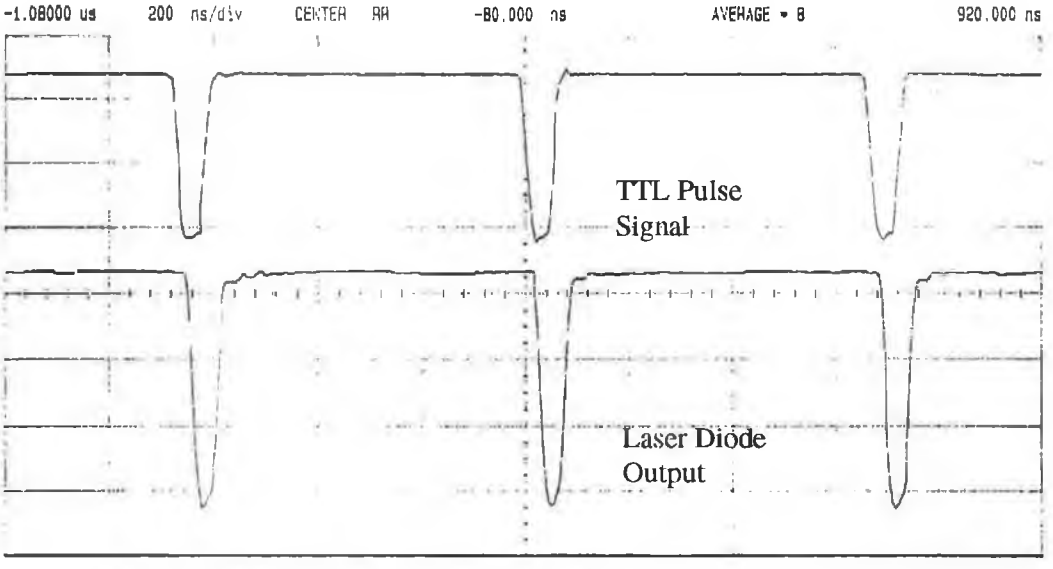

Figure 5.4 Timing diagrams for the laser diode pulsing unit and corresponding Laser diode output

figure 5.4 timing diagrams for the laser diode pulsing unit and the corresponding pulse waveforms are shown for 50ns pulses at a repetition rate of 1.5 MHz. A pigtailed photodiode (App. 3) along with a 250 MHz Hewlett Packard 54510A digitising Oscilloscope was used to detect the back-scattered signal from the sensing fibre. The photodiode has integral amplification with a rise time of 14ns along with a typical response of 4mV per μW. Approximately 30% of the laser diode intensity (~3mW) could be launched into the core of the telecommunication fibre using a 0.22 N.A. microscope objective lens. Therefore, for a three sensor system, as shown in figure 5.5 , assuming a reflection of 4% from the sensing points, 3 pulses of approximately 3.75μ W should be recorded from the fibre ends.

The overall response time (and therefore spatial resolution) of the system was thus mainly dependent on the laser diode pulse width. Unfortunately spatial resolutions in the

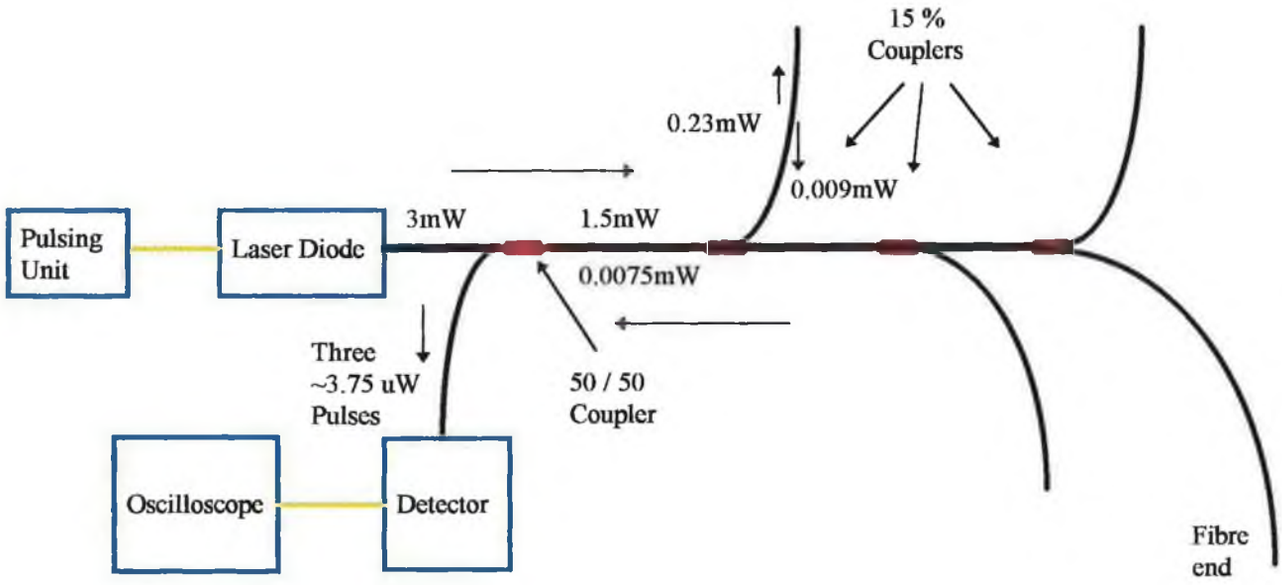

Figure 5.5 Quasi - distributed fibre optic sensor network using constructed 675nm OTDR. The theoretical power values at all points in the network are shown. Assuming a fresnel reflection of 4% and neglecting fibre attenuation, 3 pulses of approximately 3.75μ W should be recorded from the 3 fibre ends.

order of metres can not be achieved with the type of laser diode used here. This is because the laser diode is designed for CW use, i.e. the current is regulated to prevent the device from overheating. This is opposed to pulsed laser diode systems which draw a large current in a short time period. In this case, overheating is avoided since the device is on for only a few ns. However, at present, the cost of pulsed laser diode systems can run into several thousands of pounds and as a result, their use, was not feasible in this work.

5.5 DISTRIBUTED SENSING RESULTS

5.5.1 Commercial 850nm OTDR

The first objective in developing a distributed sensor system using a commercial 850nm OTDR is the selection of an appropriate sensor dye which absorbs in this spectral region. Such a dye (Trimethinecyanine)[8] was provided by Dr. P. Czerney of the Institut fur Physikalishe Chemie, Friedrich-Schiller-Universitat, Jena, Germany. The absorption spectrum of this dye dissolved in iso - propanol is shown for varying pH in figure 5.6. However the spectral properties of this dye were completely destroyed when it was immobilised in a sol-gel matrix. Initially it was expected that the low pH environment of the conventional (pH 1) sol gel recipe was too harsh for the dye. However repeated attempts at more basic pH values yielded similar results. The dye was next immobilised in a range of polymers including polyvinylchloride (PVC), polymethylmethacrylate (PMMA) and silicone. For the range of polymers tested, absorbance spectra with maxima centered around 850 nm were recorded, but in all cases the absorbance was barely affected, if at all, by pH variation. A range of other NIR dyes were then investigated but similar immobilisation problems were encountered.

Due to the difficulties in immobilising the Trimethinecyanine dye, investigations were carried out with the dye in solution phase in a variant of the immobilisation configuration proposed earlier. Each of the fibre ends were placed into a iso-propanol / near infrared (NIR) dye solution. A small mirror was then positioned less than a mm from the fibre ends,so as to return light for detection. In such a way, the light interrogated

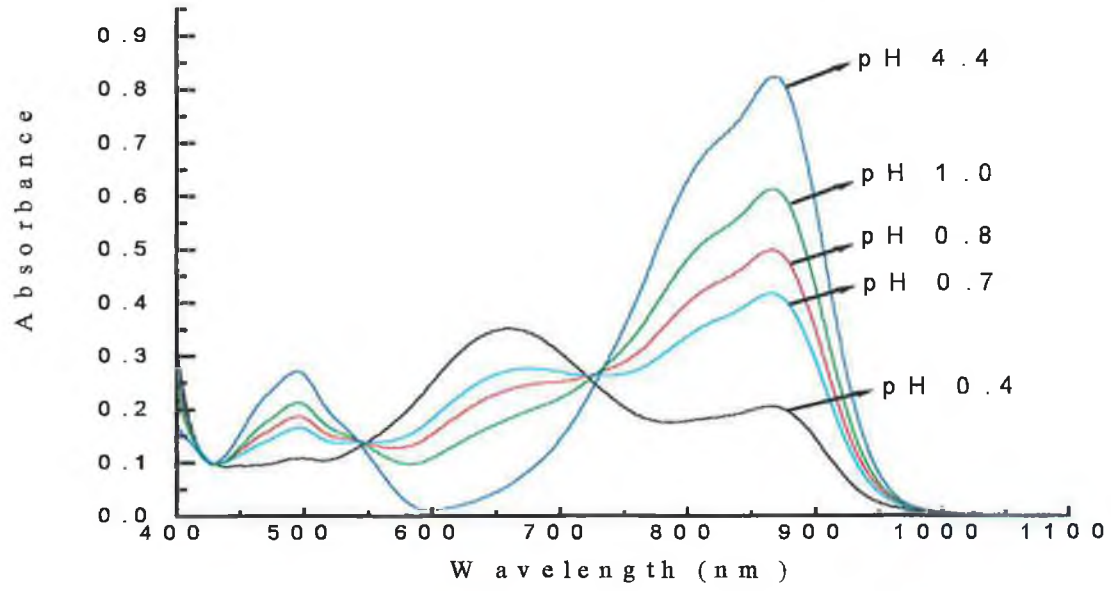

Figure 5.6 Absorption spectra of NIR dye dissolved in iso-propanol for varying pH

a short distance of the NIR dye solution. The pH was then varied by adding HCl to the solution. The attenuation was monitored as a function of pH for each of the three sensing points using the commercial OTDR. In this experiment 5ns pulses were launched into the fibre giving a spatial resolution of approximately 1 metre. Figure 5.7 shows the reflected signal from one of the sensor points located 190m from the source for a range of pH values. The response can be seen to be consistent with that shown in figure 5.6. Although the pH resolution was not determined exactly, it is clearly less than 0.05 pH units over the pH range 0.4 to 1.0. In figure 5.8, OTDR traces for 3 sensor points separated by 100m are shown. The upper trace shows the response of the system to 3 different pH values at the three sensor locations. The lower trace, which is displaced for clarity, is used for referencing purposes. The initial spike in each trace corresponds to the fresnel reflection from the fibre proximal end while the reflection from the end of the fibre

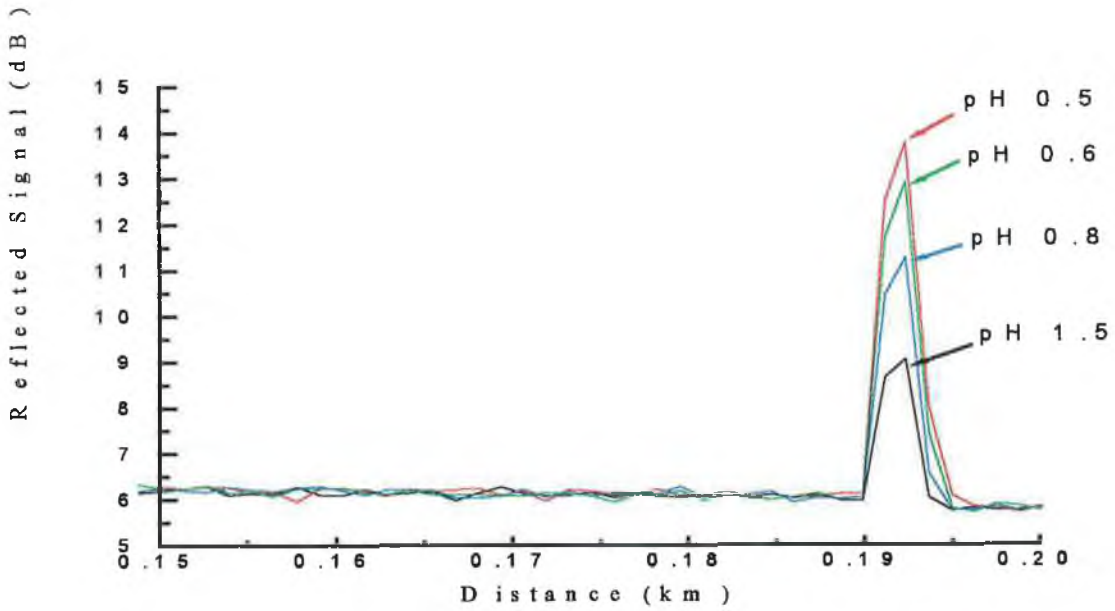

Figure 5.7 Reflected signal as a function of pH from one of the sensing points

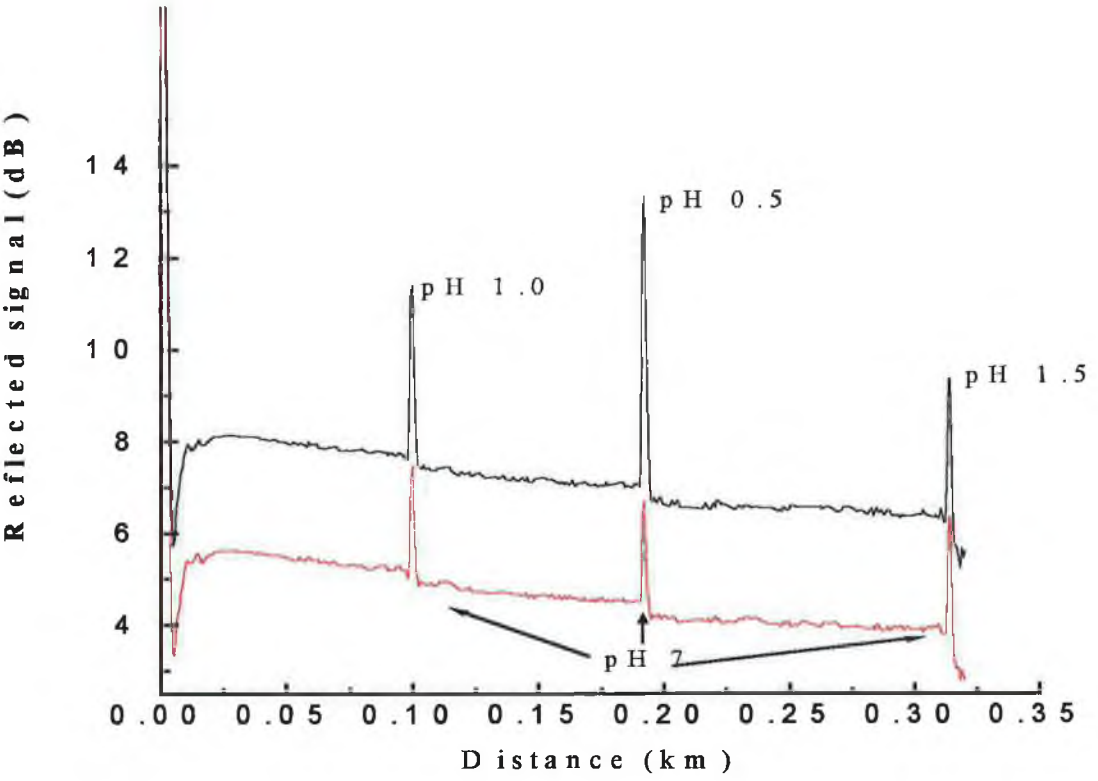

Figure 5.8 Reflected signal Vs. pH for 3 sensing points separated by approximately 100m. The lower trace which is used for referencing is displaced for clarity.

is not shown. These preliminary data clearly demonstrate the potential of this approach for multipoint/quasi distributed sensing. Thus, the difficulty that has arisen, in immobilising the NIR dye in a sol gel or polymer matrix is the only apparent factor which is limiting the further development of this approach in a quasi-distributed sensing system.

5.5.2 670nm OTDR

As discussed in section 5.4.2, an OTDR operating at 670nm was constructed. The system had a pulse width of 50ns leading to a spatial resolution of approximately 10 metres. Analysis of the backscattered light was carried out using a 14ns rise time photodiode and a 250MHz Hewlett Packard digitising oscilloscope. Initially, the system was used to interrogate a fibre length of ~30m using the setup shown in figure 5.9. The resulting oscilloscope output is shown in figure 5.10. The first feature corresponding to the reflection from the 15% coupler was used to signify the starting point of the fibre. The second feature in the output corresponds to the reflection from the fibre end. The propagation delay between the initial pulse and reflections from the fibre thus enables an optical picture to be created in the time domain of the fibre under test. The fibre end was now placed into a oxazine / methanol solution repeating the experiment discussed in

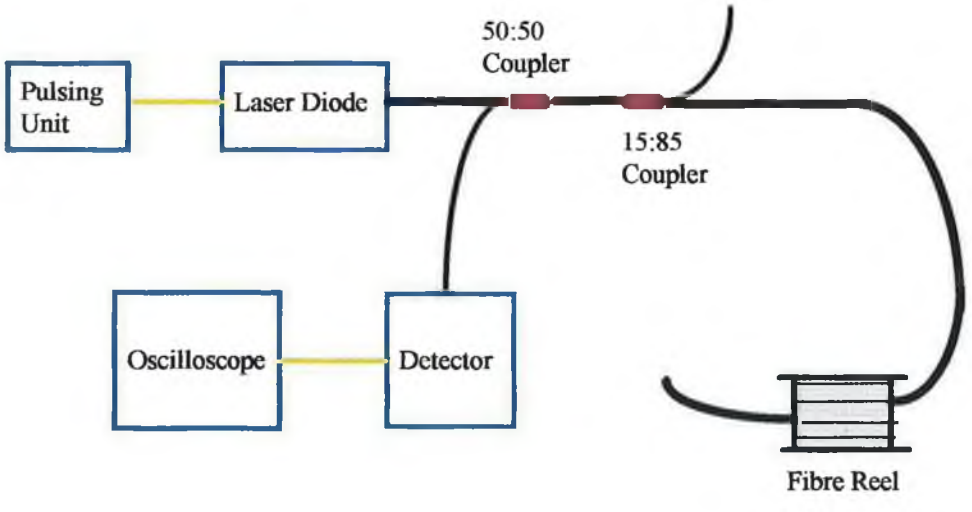

Figure 5.9 670nm OTDR system

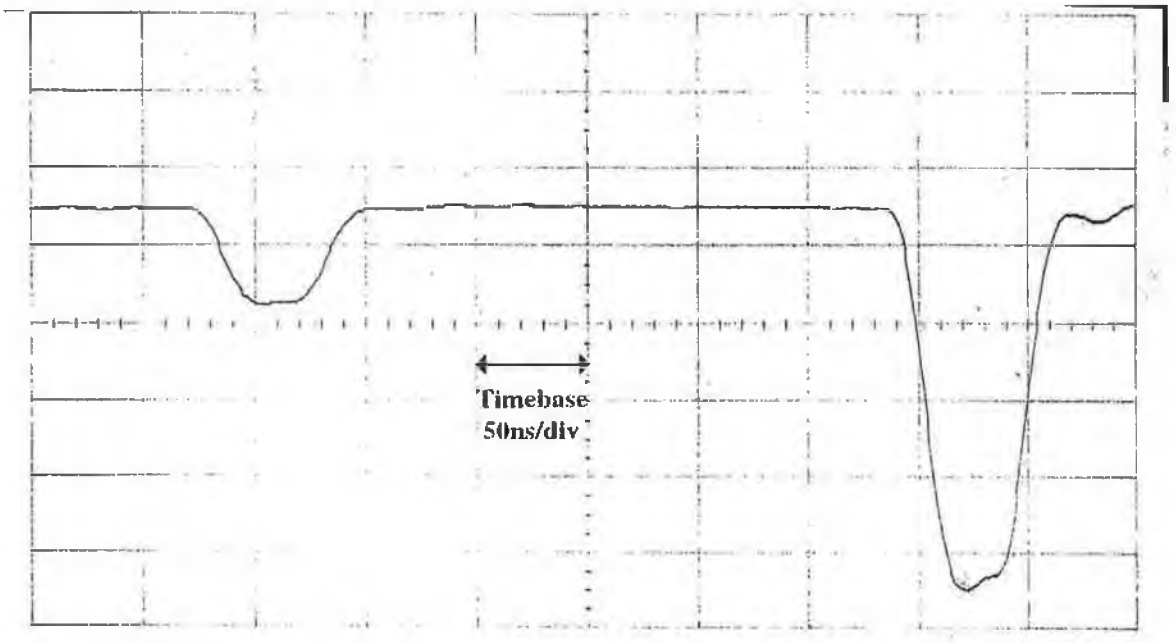

Figure 5.10 Backscattered signal from a 30m length of fibre using a 670nm OTDR system

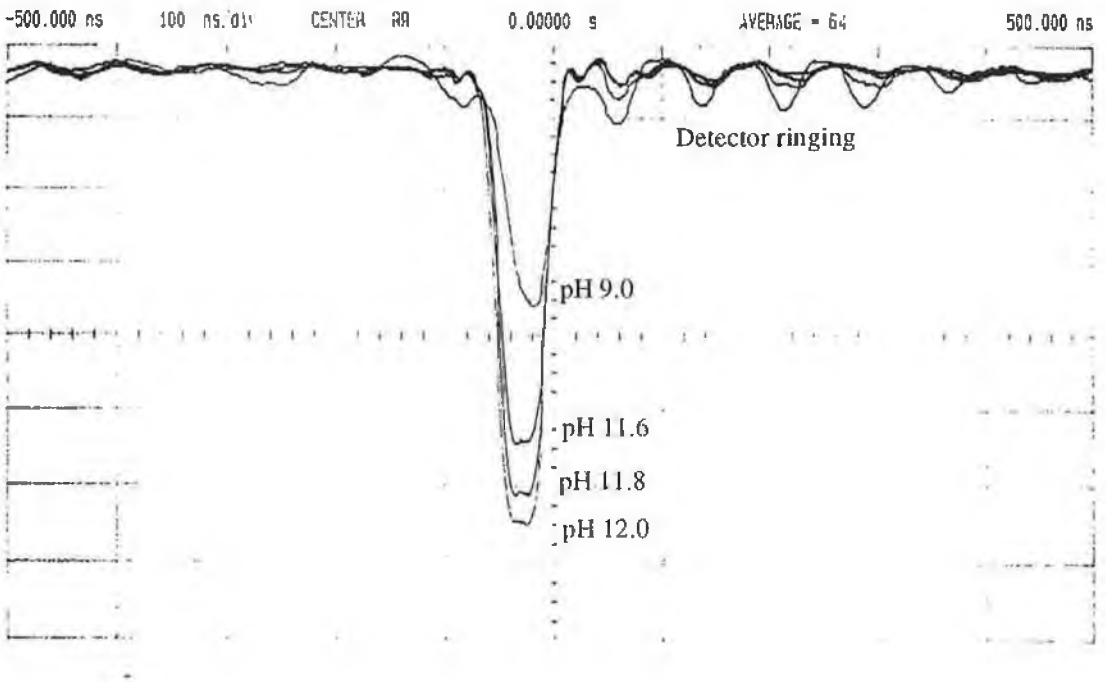

Figure 5.11 Reflected signal from fibre end as a function of pH.

section 5.5.1. A mirror was again used to return light for detection. As mentioned earlier, oxazine is an ammonia and pH sensitive dye. It exhibits highest sensitivity over the pH range 10-12. The effect of varying the pH on the reflected signal is shown in figure 5.11. The reflected intensity can be seen to increase by a factor of 2 over the pH range 9-12. The next step in developing an quasi-distributed chemical sensor using the 670nm OTDR system was the immobilisation of the oxazine dye onto the fibre tip. However when this was carried out the reflected signal was not discernible above the noise of the system. This was due to a combination of the following factors (i) the attenuation of telecom fibres increases significantly with decreasing wavelength e.g. the attenuation at 670nm was measured to be 18.5 dB/km, compared to around 3dB/km at 850nm, (ii) the intensity of the laser light launched into the fibre was too low and (iii) the poor optical efficiency of this sensing configuration. Thus, to successively implement a quasi-distributed system at this wavelength, a higher intensity laser diode is required along with optimisation of the immobilisation technique.

5.6 CONCLUSION

In this chapter, preliminary results leading to the development of a quasi-distributed chemical sensor system using a commercial 850nm and a constructed 670nm OTDR have been presented. A number of issues, however, need to be addressed to further the development of this sensing technique. Firstly, the identification of a range of suitable NIR dyes that are compatible with sol-gel or polymer immobilisation is required. Secondly, the immobilisation method needs to be optimised so as to maximise the return signal from the fibre cavity. This could be achieved by introducing scattering centres into the sol-gel silica thereby increasing the amount of scattered light received from the fibre tip. Finally, to further develop a 670nm OTDR, a higher intensity laser diode is required to overcome problems associated with the fibre attenuation and the low intensity signal obtained from this sensing configuration.

REFERENCES

1. R.A. Lieberman, L.L. Blyler, L.G. Cohen. **"Distributed fluorescence oxygen sensor"** Proc. Optical fibre sensors (Jan 27-29 1988) New Orleans 346-347.

2. G. O Keeffe, B.D. MacCraith, A.K. McEvoy, C.M. McDonagh, J.F. McGilp. **"Development of a LED-based phase fluorimetric oxygen sensor using evanescent wave excitation of a sol-gel immobilised dye"** Sensors and Actuators B 29 (1995) , pp.226-230.

3. C. Klimcak, G. Radhakrishnan, S. Delcamp, Y.Chan, B Jaduszliwer, S. Moss **"Development of a fiber optic chemical dosimeter for use in the remote detection of hydrazine propellant vapor leaks at Cape Canaveral air force station"** Proc. SPIE Vol. 2293, Chemical, Biochemical, and Environmental fibre sensors VI (26-27 July 1994) San Diego, pp.209-215.

4. A. Kharaz, B.E. **Jones "A distributed optical-fibre sensing system for multi-point humidity measurements"** Sensors and Actuators A 46-47(1995), pp. 491-493.

5. J.M. Senior **"Optical fibre communications : Principles and practice" (Second Edition)** Prentice Hall (1995).

6. G. O'Keeffe **"Development of fibre optic evanescent-wave fluorescence-based sensors"** Ph.D. Thesis (1995) Dublin City University.

7. EXFO-FCS-100 OTDR operating manual.

8. H. Lindauer, P Czerney, G.J. Mohr, U.W. Crummit. **"New near infrared absorbing acidochromic dyes and their application in sensor techniques"** Dyes and Pigments, Vol. 26, (1994), pp.229-235.

CHAPTER 6

CONCLUSION

The work presented in this thesis described a novel immobilisation approach for analyte-sensitive reagents for point sensing and quasi-distributed sensing applications. The sensing configuration was achieved by means of selective fibre etching and sol-gel immobilisation techniques. The sensor configuration was evaluated initially for point sensing applications using both fluorescence and absorption-based indicators. A pH - sensitive NIR dye compatible with a commercial OTDR was used to demonstrate the suitability of this approach for multi-point sensing.

A carbon-dioxide sensor based on evanescent-wave excitation of a pyranine dye encapsulated in a thin microporous coating fabricated by the sol-gel process was also presented. The sensing process was based on the quenching of fluorescence from the pyranine molecules in the presence of carbon dioxide. The sensor was found to be temporally unstable due to the relationship between sensor output and film water concentration.

The characterisation of a relatively new family of materials known as organically modified silicates (ormosils) was also carried out. It was found that the introduction of the organic component increased the critical thickness of sol-gel thin films along with improving the temporal stability of the films. The porosity of the sol-gel films was also found to be affected by introducing an organic component. This was observed by monitoring the microstructure of the films as a function of organic : inorganic precursor ratio using FTIR spectroscopy.

Further work based on the results presented here should initially concentrate on the identification of a range of stable NIR dyes compatible with a 850nm OTDR. While laser diodes are soon expected to be available in the blue/green region of the spectrum, the high attenuation of optical fibres in this spectral region would make that approach impractical. Optimisation of the immobilisation method needs also to be addressed. While

the sol-gel-derived silica adheres well to the core of the optical fibre, the immobilisation procedure is lenghty and difficult to reproduce. A new immobilisation technique known as photo-initiated polymerisation might yield more reproducible results. Finally the development of a dual wavelength OTDR system, which would offer the possibility of inherent referencing is also of interest.

APPENDIX A LED driver and Lockin detection circuitry

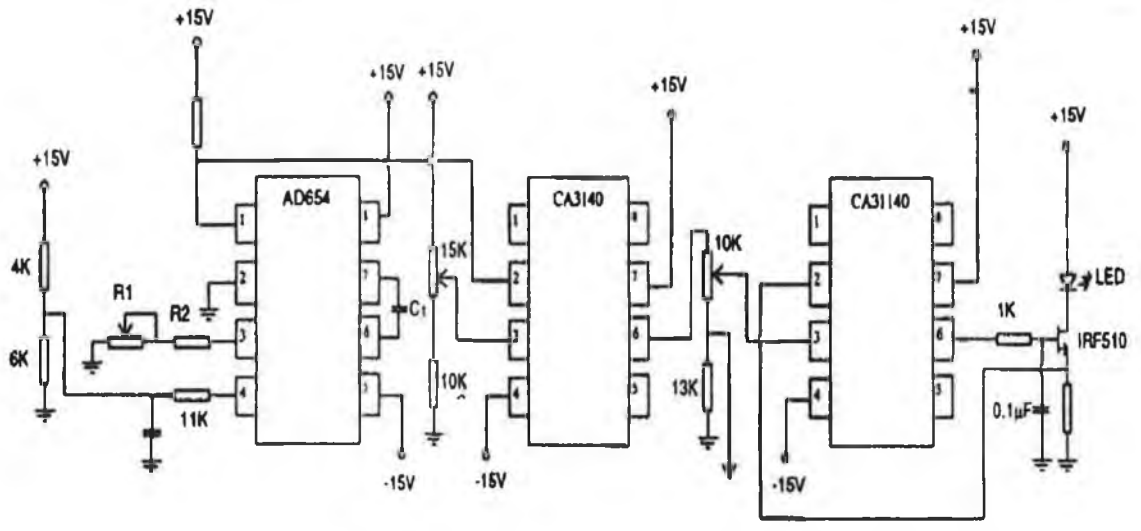

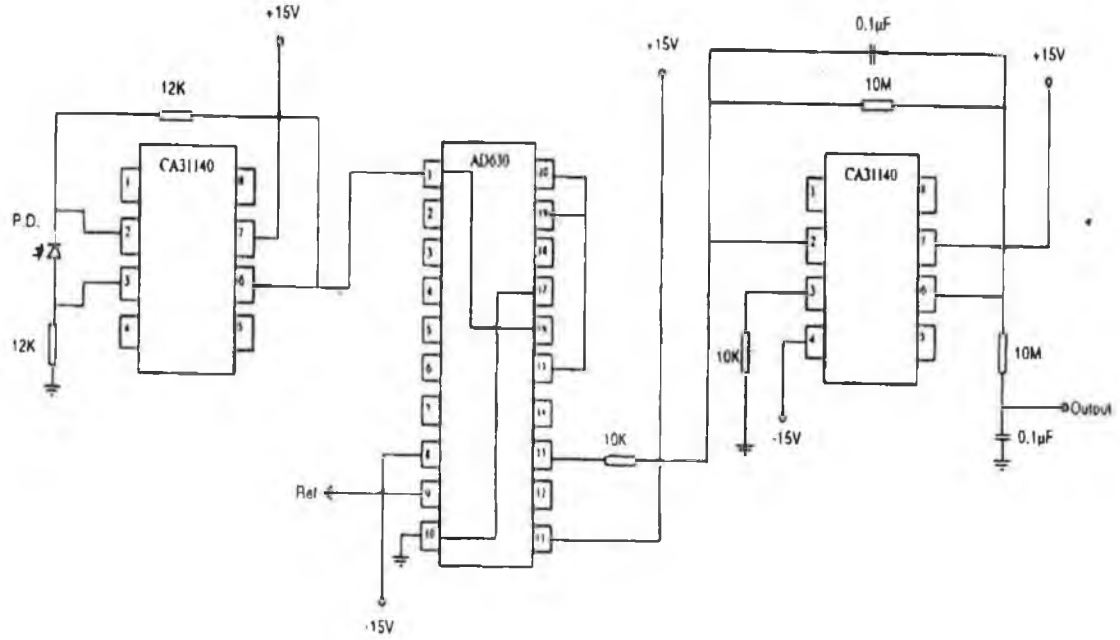

APPENDIX B **Laser diode pulsing circuitry**